JOURNAL OF GEOPHYSICAL RESEARCH, VOL. 99, NO. B10, PAGES 19,975–20,010, OCTOBER 10, 1994

Deformation across the western United States: A local estimate of Pacific–North America transform deformation

Eugene D. Humphreys and Ray J. Weldon II

Department of Geological Sciences, University of Oregon, Eugene

Abstract. We obtain a locally based estimate of Pacific-North America relative motion and an uncertainty in this estimate by integrating deformation rate along three different paths leading west across southwestern North America from east of the Rio Grande Rift to near the continental escarpment. Data are primarily Quaternary geologic slip rate estimates, and resulting deformation determinations therefore are "instantaneous" in a geologic sense but "long term" with respect to earthquake cycles. We deduce a rate of motion of the Pacific plate relative to North America that is 48 ±2 mm/yr, a rate indistinguishable from that predicted by the global kinematic models RM2 and NUVEL-1; however, we obtain an orientation that is 5–9° counterclockwise of these models. A more westerly motion of the Pacific plate, with respect to North America, is calculated from all three paths. The relatively westerly motion of the Pacific plate is accommodated by deformation in the North American continent that includes slip on relatively counterclockwise-oriented strike-slip faults (including the San Andreas fault), which is especially relevant in and south of the Transverse Ranges, and a margin-normal component of net extension across the continent, which is especially relevant north of the Transverse Ranges. Deformation of the SW United States occurs in regionally coherent domains within which the style of deformation is approximately uniform. In the vicinity of the Transverse Ranges, two important shear systems splay from the San Andreas fault: the eastern California shear zone trending NNW from the eastern Transverse Ranges and the trans-Peninsular faults trending SSE from the western and central Transverse Ranges. Within the Transverse Ranges the right-lateral San Andreas fault steps left, seemingly requiring large amounts of convergence there. However, most of this convergence is avoided through a "funneling flow" of the crust toward the western Transverse Ranges and into the relatively narrow central California Coast Ranges and the northern motion of the Mojave. The former process involves an alternation of rotation direction from counterclockwise (in and south of the central Transverse Ranges) to clockwise (in the western Transverse Ranges).

Introduction

The occurrence of broadly distributed young faulting in the western United States (Figure 1a) affords an opportunity to study the process of continental transform deformation in a well-studied region. Essential to such a study is an understanding of the regional kinematics of this broadly distributed and diverse deformation field. An important aspect is knowledge of the far-field plate motions that fundamentally drive transform deformation. Previous kinematic models of the southwestern United States have been constructed so that the total deformation across the region is consistent with global kinematic models such as RM2 [*Minster and Jordan*, 1978] or NUVEL-1 [*DeMets et al.*, 1990]. In order to keep regional plate margin kinematics consistent with the globally derived Pacific-North American plate velocity, these models included unrealistically great deformation rates somewhere in the southern California region. The models of *Hill* [1982] and *Bird and Rosenstock* [1984] include excessive convergence rates across the length of the Transverse Ranges. *Weldon and Humphreys* [1986] introduced a model that has relatively low convergence rates across the central and eastern Transverse Ranges and high convergence rates across the western Transverse Ranges by including relatively high rates of strike-slip faulting and a E-W oriented shortening in the continental borderland. They also included no deformation east of the San Andreas system south of the Garlock fault. *Saucier and Humphreys* [1993] and *Humphreys and Weldon* [1991] included deformation east of the San Andreas fault and still found that NUVEL-1 boundary conditions resulted in margin-normal contraction.

In this paper we consider the deformation encountered along three paths leading from the North American

Paper number 94JB00899.
0148-0227/94/94JB-00899$05.00

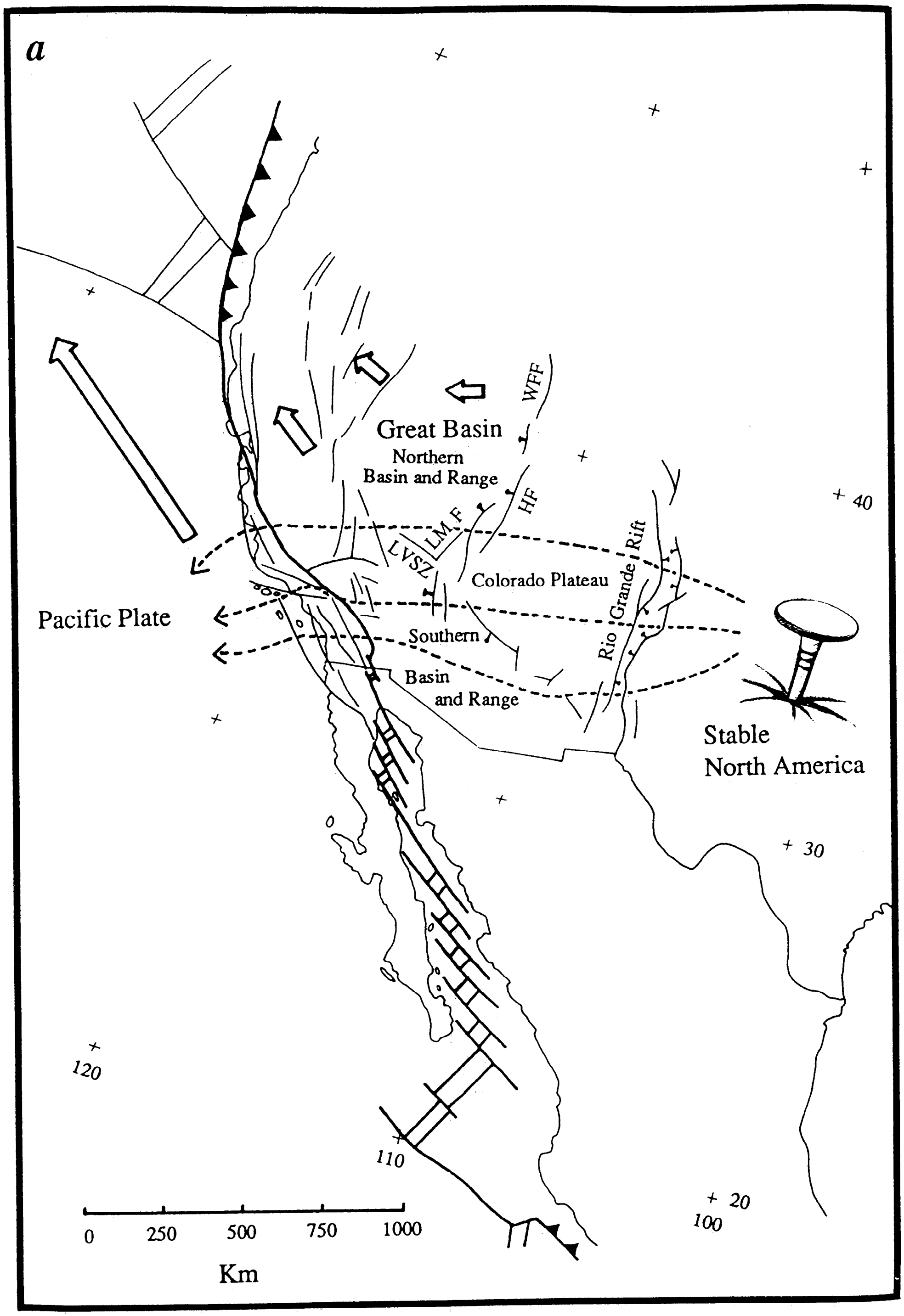

Figure 1. Fault map of areas crossed by the three paths of integration across the Pacific-North America boundary. (a) The deforming SW United States and adjacent regions. Heavy lines represent the most important faults that accommodate relative plate motion, and lighter lines represent other faults. Paired parallel lines are spreading centers. Bars are on downthrown sides of normal faults. Three paths are shown leading from stable North America to the Pacific plate. Arrows indicate velocity with respect to stable North America. Map symbols are HF, Hurricane fault; LMF, Lake Mead fault; WFF, Wasatch Front fault; and LVSZ, Las Vegas shear zone. (b) Fault map of the southern California region. Projection is oblique Mercator projection about the RM2 Pacific-North America pole [*Minster and Jordan*, 1978] (which is indistinguishable from the projection about the NUVEL-1 Pacific-North America pole [*DeMets et al.*, 1990]). Map abbreviations are BPF, Big Pine fault; CBF, Coronado Bank fault; ECSZ, Eastern California shear zone; FCF, Furnace Creek fault; HMF, Hunter Mountain fault; IF, Imperial fault; LSF, Laguna Salada fault; N-IF, Newport-Inglewood fault; NDVF, Northern Death Valley fault; OVF, Owens Valley fault; PVF, Panamint Valley fault; RCF, Rose Canyon fault; SBM, San Bernardino Mountains; SDTF, San Diego Trough fault; SDVF, Southern Death Valley fault; SGF, San Gabriel fault; SGM, San Gabriel Mountains; SGP, San Gorgonio Pass; SIF, San Isidro fault; SMB, Santa Maria Basin; SMF, San Miguel-Vallicitos fault; SSF, San Simeon fault; SYF, Santa Ynez fault; and VB, Ventura Basin.

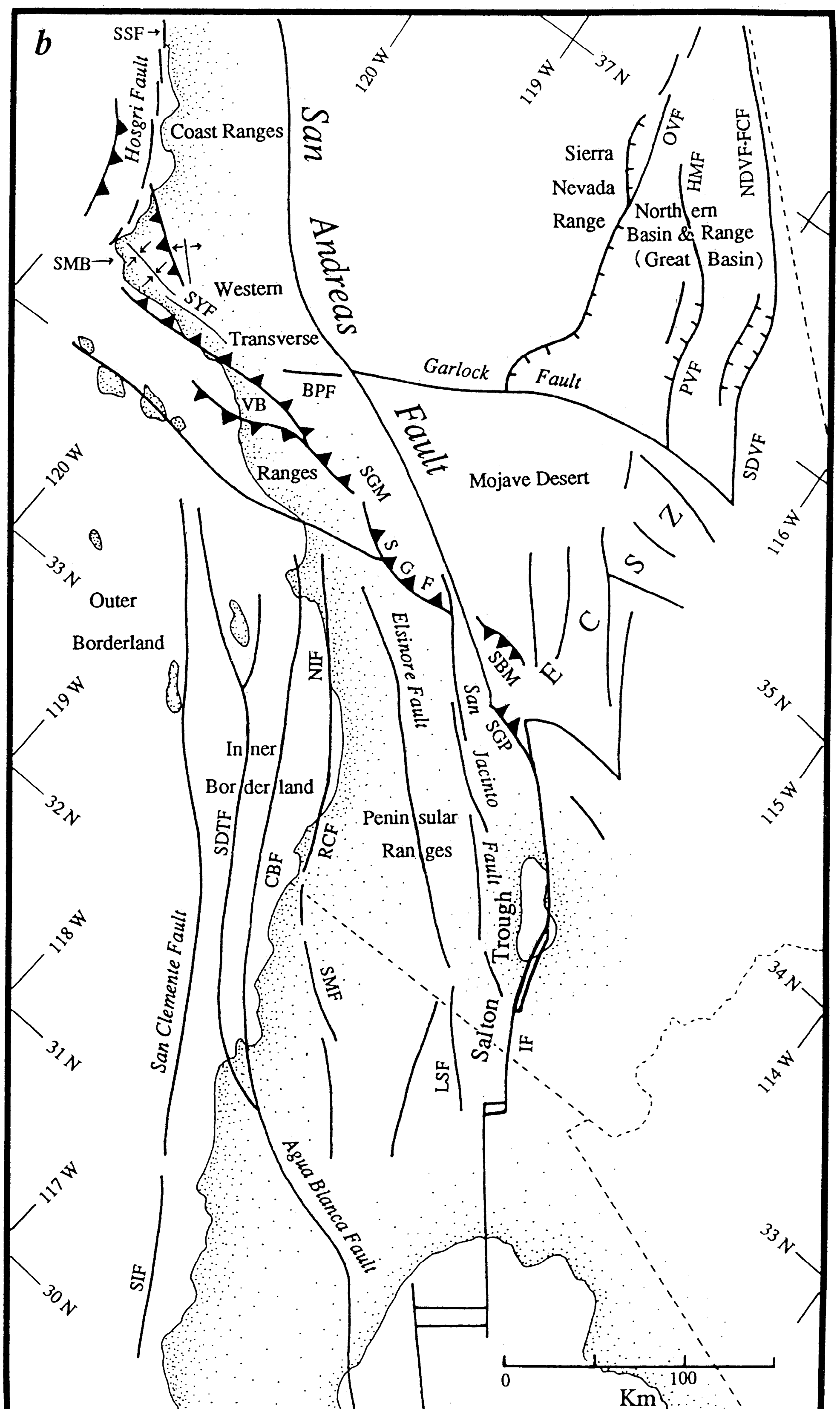

Figure 1. (continued)

interior to the Pacific plate (Figures 1a and 2). In doing so, we obtain both a description of the transform-accommodating deformation and a locally based estimate of Pacific-North America plate motion. The estimate of relative plate motion that we obtain is independent of global kinematic models, and the precision of our estimate is comparable to that offered by the presently available global kinematic models RM2 and NUVEL-1. We obtain a velocity field that avoids high (~1 cm/yr) convergence rates both in the central to eastern

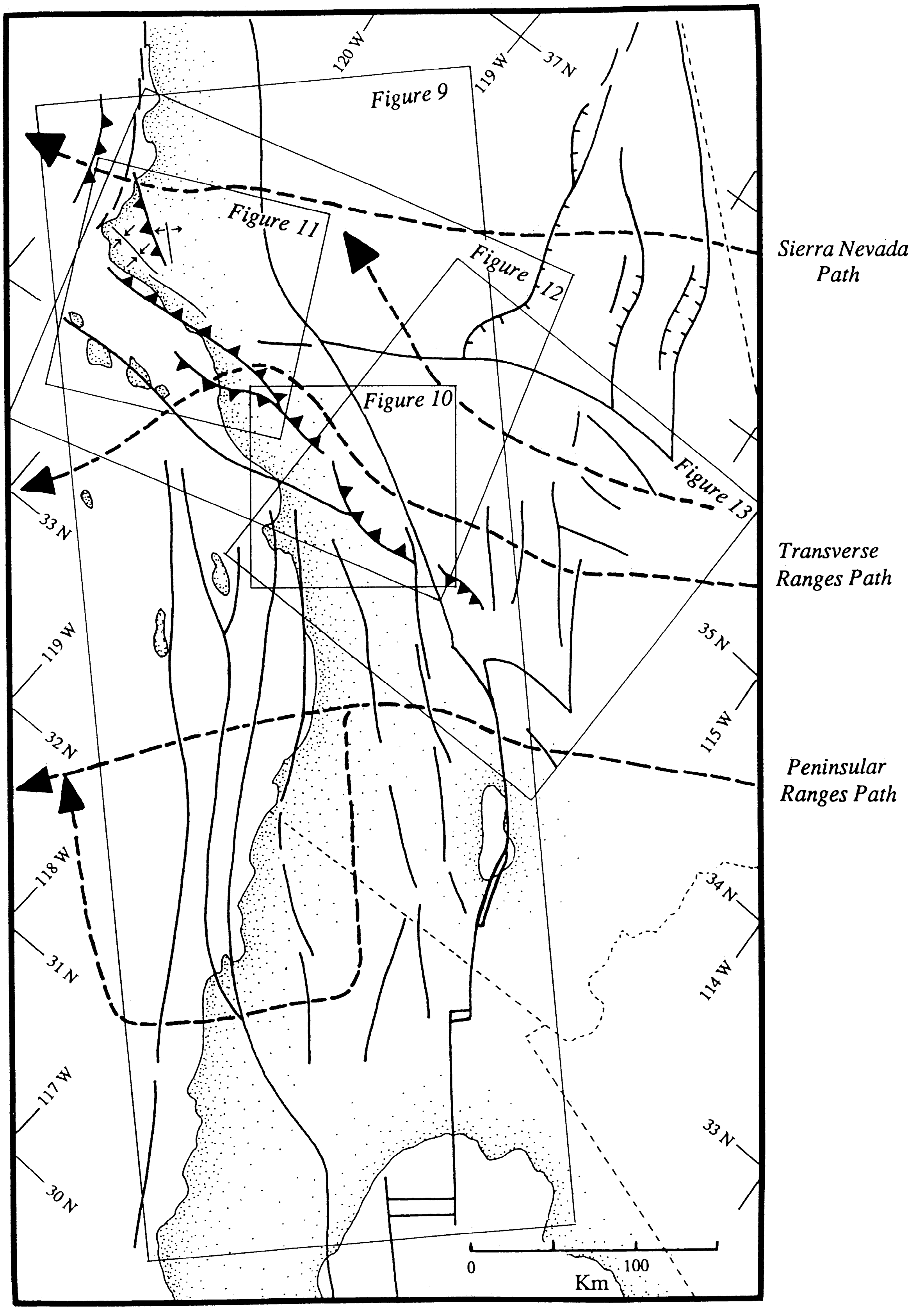

Figure 2. Southern California index map. Shown are the three paths (and their subpaths) used in integrating deformation to obtain our locally based Pacific-North America relative velocity estimate. Also shown are the areas of Figures 9-13.

Transverse Ranges and in the offshore region by having the Pacific plate move more westerly, relative to North America, than is derived from the global models, and by including regional rotations and a greater role for faulting east of the San Andreas fault.

Description of Method

The relative motion between two points can be found by integrating velocity changes along the length of an arbitrary path connecting the two points [*Minster and Jordan*, 1984]. In practice, this calculation usually involves a summation of deformation rates for known active faults encountered along the chosen path [e.g., *Weldon and Humphreys*, 1986]. Integration also should include velocity gradients across rotating rigid blocks and across regions of continuously distributed deformation. If a complete accounting is made of all velocity changes encountered along any chosen path, then the velocity calculated at the end of the path gives the correct relative motion between the two points. This is true regardless of the nature of the deformation field away from the path, either on the surface of the Earth or beneath its surface.

Our path choices (Figure 2) are guided by the availability of data, by an attempt to avoid controversial regions and regions of exceptionally complex or distributed deformation, and by a desire to make use of strike-slip faults where possible. Strike-slip faults are emphasized because their slip vector orientations usually are better constrained than those associated with other deformational styles. Furthermore, because the zone of deformation between the Pacific and North America plates is principally one of simple shear, strike-slip faults best typify the regional deformational style. Where different regions deforming by simple shear adjoin, an activation of additional slip systems, required by the von Mises criterion [e.g., *Hirth and Lothe*, 1982], results in a region of more complex deformation. We attempt to avoid complexly deforming regions; however, broadly distributed deformation and the rotation of large blocks are explicitly included in our integration, where encountered.

Rotations are especially difficult to recognize because they are not easily associated with discrete fault boundaries; rather, their velocity contributions occur over the portions of paths that are located on the rotating block. To recognize block rotation, we must have either high quality paleomagnetic data that indicate regionally consistent young rotation or an understanding of the kinematics in a region greater than that addressed along a path. Because rotations are difficult to recognize (or dismiss) and are difficult to characterize uniquely, the uncertainties introduced by their possible presence must be handled carefully. Here we argue their presence (or absence) mainly on local kinematic grounds and use paleomagnetic data to help quantify rates where such data are available and consistent. We deduce that kinematically important rotations occur in several regions, and that they are not important in other regions.

To avoid complications associated with changes in kinematic style on time scales longer than hundreds of thousands of years and as short as the seismic cycle, which is hundreds to thousands of years, data are chosen to emphasize late Quaternary slip rates (tens of thousands of years). In the absence of such data we use longer-term slip rate estimates, and in lieu of reliable geologic data, we consider geodetic data. Where geodetic data are used, care is taken to avoid the elastic strain field near major faults. This priority in data selection is motivated by a desire for maximum consistency.

An important aspect of this analysis is a formal inclusion of uncertainty. To describe the uncertainty associated with each structure encountered along the length of a path, we ascribe probability functions to the rate and orientation chosen for that structure. If velocity data for active structures encountered along a path are independent of one another, the probability function describing total motion encountered along the path can be determined by convolving the probability functions for each of the features considered. Because independent velocity estimates can be determined for several paths joining two points, we can combine the individual-path estimates of relative velocity by taking the product of their end-of-path probability functions to provide a better estimate of the relative velocity between two points. If data from each path are not completely independent from one another, the estimated probability function for the product will tend to be too narrow. Therefore we have chosen paths joining the North America and Pacific plates for which the data are nearly independent. However, inferences about the rates and styles of individual structures often are influenced by comparison with similar structures or kinematic relationships between structures. Indeed, few geologic data are truly independent. For example, the late Cenozoic rotation of the Colorado Plateau is commonly inferred from the southward increase of activity across the Rio Grande Rift, and thus different paths that cross the Colorado Plateau and Rio Grande Rift are not independent. Because of such interdependence, systematic biases may enter into the analysis. We attempt to minimize this bias by chosing conservative (i.e., relatively large) uncertainty estimates and by using paths that cross structures of different orientations and, often, completely different styles. The fact that each of our three paths yields a similar result, despite crossing the San Andreas fault zone where its trend, rate, and associated deformation differ in both magnitude and style attests to the robustness of the technique and the overall quality of the data.

To describe uncertainties associated with tectonic features encountered along a path, we create asymmetrical triangular-shaped probability functions centered on the best rate and orientation estimates and decreasing to zero probability at chosen limits. We choose this distribution because it is a simple representation of the data as reported by the field researchers, i.e., a most likely estimate rate and "absolute" uncertainty limits. Other center-weighted probability distributions were tried (such as Gaussian and trapezoidal) and produced virtually identical results. While rate information typically is derived directly from the work of others, orientation information usually requires an interpretation of the style of deformation. The preferred orientation of the velocity vector associated with strike-slip faults is taken to be the fault strike at the point of crossing. To allow for the possibility that the fault trend at this site may not represent the orientation of the fault zone as a whole, or that the fault trend is oblique to the relative motion vector, we allow a range of possible orientation defined by the range of fault trend along its length near the path. The maximum excursions in fault trend are considered very unlikely orientations for slip across the entire zone, so the probability function tapers to zero at these orientations. Often we absorb into this range of possible orientations minor amounts of fault-normal deformation, either transtensive or transpressive. For instance, an assignment in orientation uncertainty of ±15° on a strike-slip fault allows for fault-normal deformation at 25% of the strike-slip rate. Where a path crosses an oblique-slip fault, an assignment of orientation is more difficult and relies on auxiliary information such as fold orientations, earthquake mechanisms, geodetic data, or theoretical results relating deformation style to oblique kinematics. Generally, we assign an orientation uncertainty of ±30° for dip-slip faults in the absence of more detailed data.

We have selected three paths, shown in Figure 2. The central of these paths, the Transverse Ranges path, is used as a reference. The other two paths are the Peninsular Ranges and Sierra Nevada paths. Table 1 lists the preferred value and limits of the rate and orientation functions that we have chosen to describe the deformation associated with each feature encountered along each path. A more detailed account of the structures encountered by the paths and pertinent references are given in the appendix.

We comment on a potential bias in the end-of-path velocity estimate that may result from a use of systematically biased uncertainty estimates. A choice of uncertainty bounds may appear, at the time of their introduction, to be simply an expression of caution. However, if one is systematically "cautious" in favoring a given direction or rate, the end-of-path velocity estimate will be affected. For example, by assigning wide limits to fault slip rates to allow a greater range of uncertainty, the assigned error can be asymmetric because negative velocities are not permitted (i.e., the sense of slip is known). To the casual reader this may simply appear as though conservative error estimates are used. However, if rates greater than the assigned best estimate are no more likely than lower rates, an end-of-path velocity estimate will have too great a velocity. As an indication of the net effect of using generally asymmetric uncertainty distributions, we show both the simple best vector sum and the end-of-path uncertainty centroid determined through convolution. Comparison of these values allows an evaluation of the effects of using asymmetric uncertainty distributions.

Two additional problems may arise when integrating over long paths. First, because the Earth is spherical, velocity varies as the cosine of distance from the Euler pole with a wavelength equal to the Earth's circumference (compared to varying directly with distance from the Euler pole for motion on a plane). In the region we consider, such effects are insignificant. For example, correcting for this effect will diminish the rate estimate of a path from the Rio Grande Rift to California (Figure 1a) by an insignificant 1.4% (0.02 mm/yr), and for deformation across California the correction is 0.05% (also ~0.02 mm/yr because of the higher rates there). These examples illustrate that the Earth can be assumed flat at the scales we are considering. Another related problem arises when the integration path traverses a rotating block whose Euler pole is poorly constrained. In particular, when path lengths are long and the Euler pole position is near and poorly constrained, significant errors may result (i.e., if the velocity is known at one point on a block, but the Euler pole position is mislocated, the velocity error accumulated in integrating to another point on the block is proportional to both the distance between the two points and the distance error in pole locations, and it is inversely proportional to both the actual distance and the assumed distance to the pole position). Because our paths traverse several blocks whose pole positions are poorly constrained, we use conservative velocity uncertainties that include pole position uncertainties.

Results of Path Integration

A summary of the rates, orientations, and uncertainties used to ascribe deformation velocities to the active faults and deformation zones are presented in the appendix. These velocities are discussed in the following three paragraphs and are summarized in Table 1 in the order they are encountered by traveling west along each of the three paths shown in Figures 1a and 2. The vector contributions of the active features encountered along each path are shown in Figures 3-7. The velocity deviations presented in this section represent the velocity range at 90% certainty. The styles of deformation in the regions represented by these paths and the resulting path products are discussed in the following sections.

Peninsular Ranges Path

The Peninsular Ranges path crosses faults that accommodate minor rates of deformation east of California: the southern Rio Grande Rift and the southern Basin and Range (Figures 1a and 3). In California, the path crosses the San Andreas fault zone south of the Transverse Ranges and crosses other NW trending strike-slip faults in southern California, northern Baja, and the continental borderland (Figures 1b and 2). West of the Elsinore fault we consider two subroutes (Figures 2 and 4): one with good orientation control (Figure 4b) that continues directly into the continental borderland and the other with better rate control (Figure 4a) that crosses the faults of northern Baja California and then continues north in the borderland to the end location of the first subroute. The end-of-path result, at 52 ±6 mm/yr N48°W ±2°, is the best constrained orientation estimate of the three paths shown in Figure 3. As shown in Table 2, this orientation is ~7° more westerly than that predicted by NUVEL-1 [*DeMets et al.*, 1990] or NUVEL-1A (DeMets et al., Effect of recent revisions to the geomagnetic reversal time scale on estimates of current plate motions, submitted to *Geophysical Research Letters*, 1994; hereinafter referred to as DeMets et al., submitted manuscript, 1994), which have formal uncertainties of about ±3° (at 90% certainty). Our more westerly orientation can be attributed directly to the relatively westerly orientation of most of the strike-slip faults encountered along this path. One means of reducing the orientation discrepancy between our model and the NUVEL-1 and NUVEL-1A models is to have greater

TABLE 1. Relative Velocities

Feature or Region		Rate, mm/yr		Azimuth, West of North	
NUVEL-1 velocity at TR path end	=>>	48.8	±3	38.7°	±3°
Net result (corrected to TR path end)	=>	48.2	±2	45.6°	±2°
Peninsular Ranges path	=>	52	±6	48°	±2°
East of the San Andreas fault	=>	1.1	+0.9-0.8	44°	±45°
Rio Grande		0.25	+0.25-0.15	90°	±30°
Southern Basin and Range		0.5	+0.50-0.25	100°	±30°
California east of the San Andreas fault		1.0	+2-1	20°	+30°-20°
San Andreas fault		30	±7	48°	+7°-3°
San Jacinto fault		12	±4	53°	+5°-10°
Elsinore fault and nearby faults to the east		5	+3-5	49°	+20°-12°
West of Elsinore	=>	5.3	±1.7	29°	+7°-9°
Northern Baja option	=>	5.5	±1.9	32°	+20°-30°
Rotation of southern California blocks		4	±4	-83°	±20°
San Miguel-Vallecitos fault zone		1	±1	55°	±8°
Agua Blanca fault		5	+3-2	67°	+10°-5°
San Isidro fault zone		2	±2	32°	±15°
Southern California option	=>	4.4	±3.0	32°	+9°-18°
Rotation of southern California blocks		3.5	±3.5	-132°	±10°
Rose Canyon fault zone		1	+2.0-0.5	37°	±7°
Coronado Bank fault zone		1	+2.0-0.5	33°	±7°
San Diego Trough fault		1	+3.0-0.5	32°	±6°
San Clemente fault		2	+5.0-1.5	46°	±5°
Transverse Range path	=>	46	±5	50°	±7°
East of California	=>	0.6	±0.5	81°	±35°
Rio Grande		0.14	+0.06-0.04	90°	±30°
Colorado Plateau rotation		0.1	±0.1	0°	±30°
Basin and Range		0.5	±0.5	90°	±30°
Mojave faults		8	+3-4	15°	±25°
San Andreas fault		36	±8	64°	±2°
Rotation of San Gabriel block		---	---	+11°	±4°
Contraction in western Transverse Ranges		11	+10-3	-10°	±20°
Left lateral in Transverse Ranges		2	±2	-85°	+10°-20°
Rotation of western Transverse Ranges		2	±2	95°	±30°
Sierra Nevada path	=>	48	±4	41°	±4°
Southern Sierra Nevada	=>	8.6	±2.0	51°	±9°
East of California	=>	2.1	+2.1-1.1	86°	±22°
Rio Grande		0.05	±0.05	90°	±30°
Colorado Plateau rotation		0.1	±0.1	0°	±30°
Great Basin east of California		2.0	+3.0-1.5	90°	±30°
California border to Sierra Nevada	=>	8.5	±1.5	57°	±8°
Great Basin option	=>	8.2	±1.8	57°	±7°
Death Valley system		1	+3-1	47°	±8°
Hunter Mtn system		3	±1	57°	±6°
Owens Valley system		1.5	+1.0-0.5	17°	+20°-13°
Mojave/Garlock option	=>	9.7	±2.5	62°	±19°
Southern Nevada fault system		1	±1	-65°	±25°
Mojave faults (from TR path)		8	+3-4	15°	±25°
Garlock fault		5	+6-2	125°	+3°-8°
Sierra Nevada block rotation		1.0	+1.0-0.5	180°	±35°
Contraction near and west of San Andreas		2	+5-1.5	-45°	+5°-15°
San Andreas fault		34	±3	41°	±4°
Right lateral west of San Andreas		6	+6-4	40°	±15°

TR is Transverse Ranges. Arrows indicate velocities calculated from subsequent values (double-headed arrow for NUVEL). Uncertainties for values with arrows are at 90% certainty.

rates of slip on borderland faults; however, as can be seen in Figure 4, increased borderland activity increases the rate discrepancy. A kinematic modification that reduces somewhat the discrepancy in both orientation and rate is an increase the counterclockwise rotation rate of the southern California blocks. The kinematic consequences of such a modification on deformation in the Transverse Ranges are discussed below.

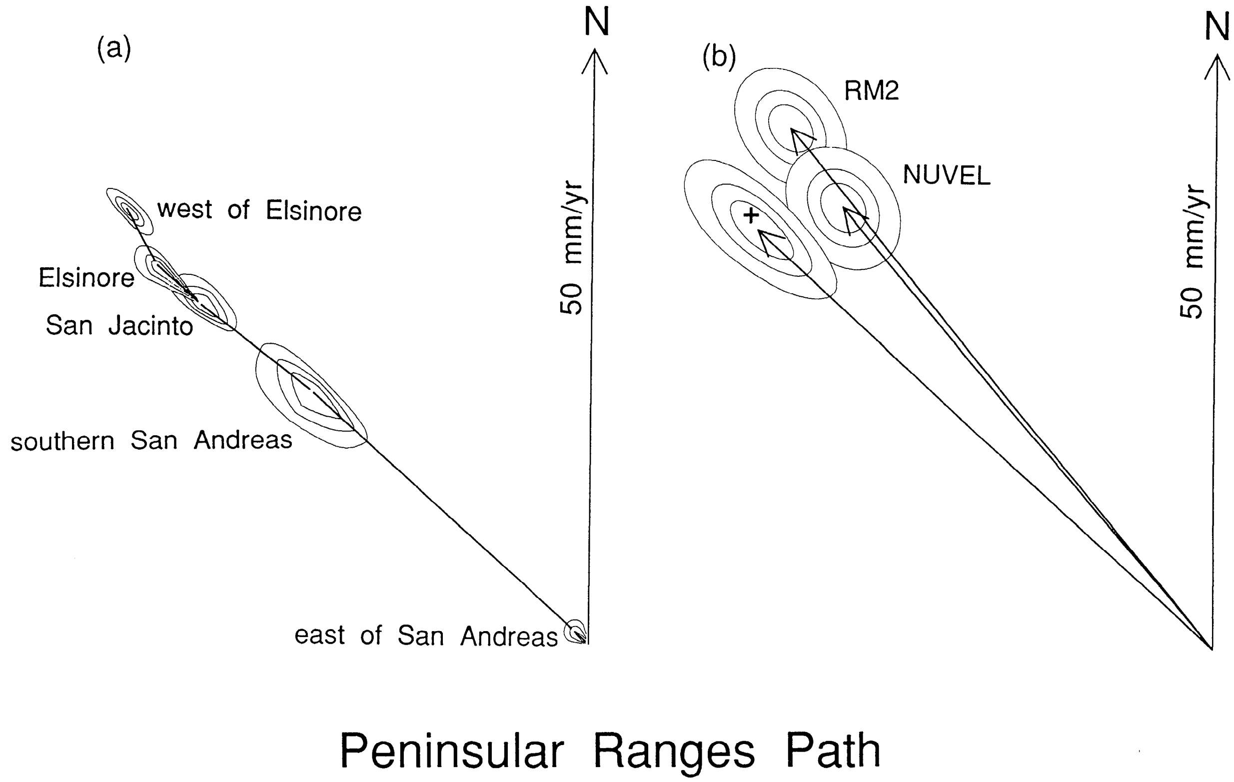

Figure 3. Vector plots for the Peninsular Ranges path. (a) The velocity data for the structures considered along the Peninsular Ranges path, shown in Figures 1a and 2. Enclosed areas about the ends of velocity vectors represent the 30, 60, and 90% confidence levels in the velocity, and vector tips lie at the most probable velocity. The north arrow represents 50 mm/yr, for scale. See Figure 4 for "west of Elsinore" estimate. (b) The end-of-path vector resulting from the convolution of uncertainty regions shown in Figure 3a, representing our estimate of Pacific-North America relative velocity derived from geologic information found along this path. Shown for comparison are the Pacific-North America velocity estimates predicted by RM2 [*Minster and Jordan*, 1978] and NUVEL-1 [*DeMets et al.*, 1990]. Although our rate estimate is indistinguishable from that of NUVEL-1, the velocity is 7° more counterclockwise in orientation. The plus symbols indicate the result of simple vector sums.

Transverse Ranges Path

Deformation east of California, including spreading in the central Rio Grande Rift, rotation of the Colorado Plateau, and Great Basin faulting in southern Nevada, contributes only minor rates (Figure 5; see appendix for details). In California, three major components contribute to the rate estimate: the "eastern California shear zone" in the central Mojave Desert [*Dokka and Travis*, 1990], the San Andreas fault zone in the Transverse Ranges, and convergence in the western Transverse Ranges fold and thrust belt. As shown in Figures 1 and 5, deformation in the Mojave and in the western Transverse Ranges contributes velocities to the path integral that are more northerly than any Pacific-North America velocity estimate, whereas the San Andreas fault, where crossed, is more westerly than any Pacific-North America velocity estimate. Because the San Andreas fault is the dominant structure encountered, the end-of-path velocity estimate is oriented with a more westerly trend relative to the globally based estimates. Accumulated deformation along this path is calculated to be 46 ±5 mm/yr N50°W ±7° compared to a NUVEL-1 predicted velocity of 48.8 mm/yr N39°W (Figure 5). Our locally based rate is indistinguishable from the NUVEL-1 and NUVEL-1A rates, whereas the orientation is different at a confidence level of greater than 95%. Uncertainties associated with deformation kinematics in the western Transverse Ranges result in end-of-path uncertainties that are greater than those obtained for the other two paths.

Sierra Nevada Path

The Sierra Nevada path (Figures 2 and 6) crosses the northern Rio Grande Rift, Colorado Plateau, the active Great Basin, the San Andreas fault in central California, regions of contraction east and west of the San Andreas, and right-lateral and contractile deformation near the California coast. We also consider an alternate eastern portion to this path (Figures 2 and 7), which passes south of the actively deforming Great Basin, crosses the Mojave Desert, and joins the main path on the Sierra Nevada block by crossing the Garlock fault. Consistency of southern Sierra Nevada motion derived from these two paths requires either a relatively inactive western Garlock fault (i.e., south of the Sierra Nevada) or the occurrence of deformation that we have not included in our calculations. Our end-of-path velocity estimate of 48 ±4 mm/yr N41°W ±4° (Figure 6) is more westerly than NUVEL-1 and NUVEL-1A by ~5° and is 1 mm/yr smaller in magnitude. The very long baseline interferometry (VLBI) station VAND, which is thought to be essentially on the Pacific plate, lies near the end of our path. Its motion relative to North America is estimated

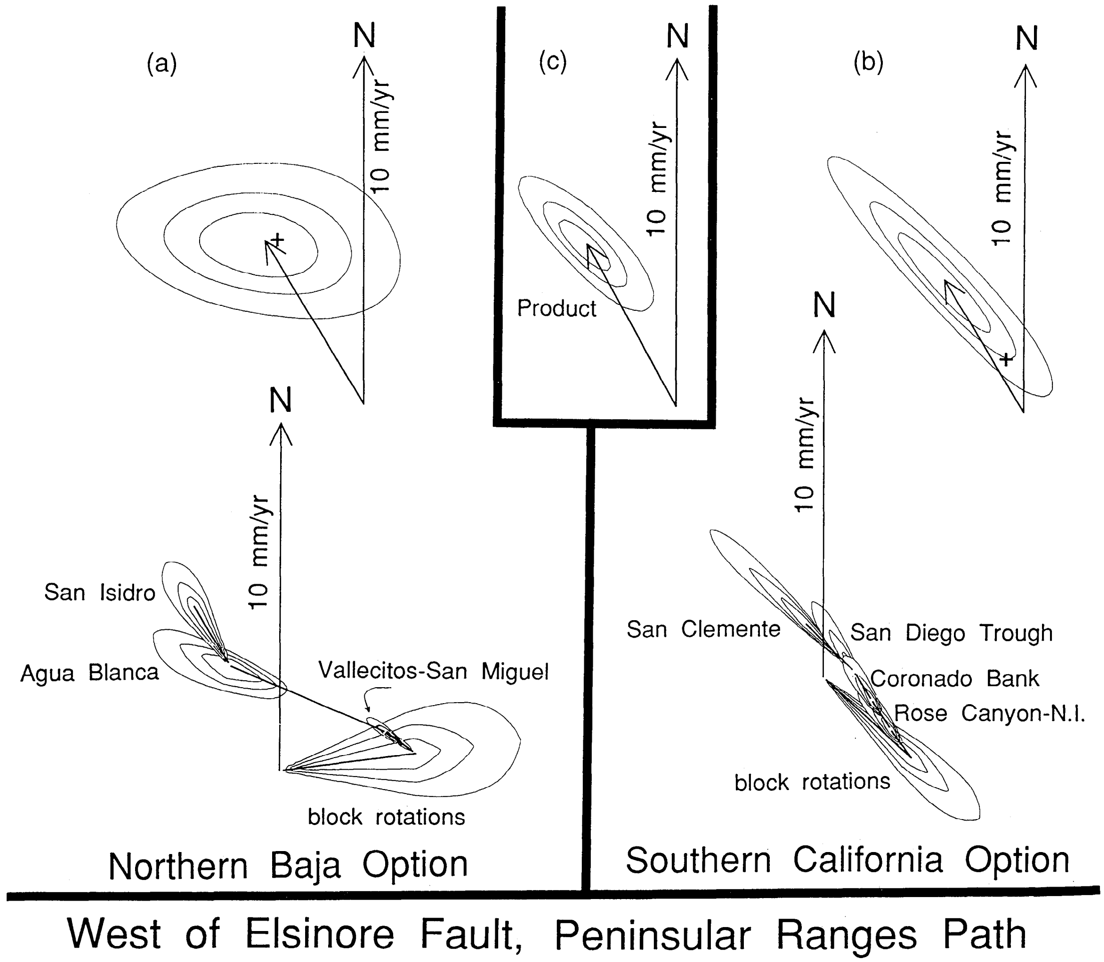

Figure 4. Vector plots for the western portion of the Peninsular Ranges path. Plot is as described in Figure 3, except scale is expanded (north arrow represents 10 mm/yr). (a) The velocity data and net convolution results for the northern Baja option. (b) The velocity data and net convolution results for the southern California option. N.I. refers to the Newport-Inglewood fault. (c) The product of the estimates from Figures 4a and 4b. This is the "west of Elsinore" estimate in Figure 3. The southern California option provides a well-constrained estimate of velocity orientation, whereas the northern Baja option provides better rate control.

at 48 ±1 mm/yr N39°W ±1° [*Ward*, 1990] and 48 ±1 N42°W ±1° [*Gordon et al.*, 1993].

Combined-Path Pacific–North America Velocity Estimate

To obtain our best Pacific-North America velocity we take the product of our three end-of-path probability functions for these three independent velocity estimates. Before doing this, however, we rotate the Sierra Nevada and the Peninsular Ranges velocity estimates by an amount needed to continue these paths to the Transverse Ranges path end. We use the NUVEL-1 pole position in making this correction (see Table 2). This correction is small, and any error introduced by potential mislocation within the NUVEL-1 pole position, including moving the pole to accommodate our velocity estimate, is very small. The product of the three end-of-path uncertainty distributions is a vector 48 ±2 mm/yr N46°W ±2° (Figure 8). This is ~7° more westerly than NUVEL-1 and NUVEL-1A.

Kinematics of Pacific–North America Interaction

In addition to providing an estimate of Pacific-North America relative motion, the deformation fields discussed for each of the paths can be used to infer the deformation of the southwest United States. As noted by *Atwater* [1970], this deformation is broadly distributed and heterogeneous in style. Figures 3, 5, and 7 illustrate that deformation in the southwest United States east of California is accommodated largely by west directed extension on normal faults and is slow compared to the deformation in California. Active systems east of California include the Rio Grande Rift, frontal faults of the Wasatch Mountains, and the western front of the Colorado Plateau. Differential motion between the areas north and south of southern Nevada are accommodated by minor rates of left-lateral strike-slip activity in southernmost Nevada. As California is approached from the east, increasing amounts of transform-related right-lateral shear are encountered. In the area of southern and

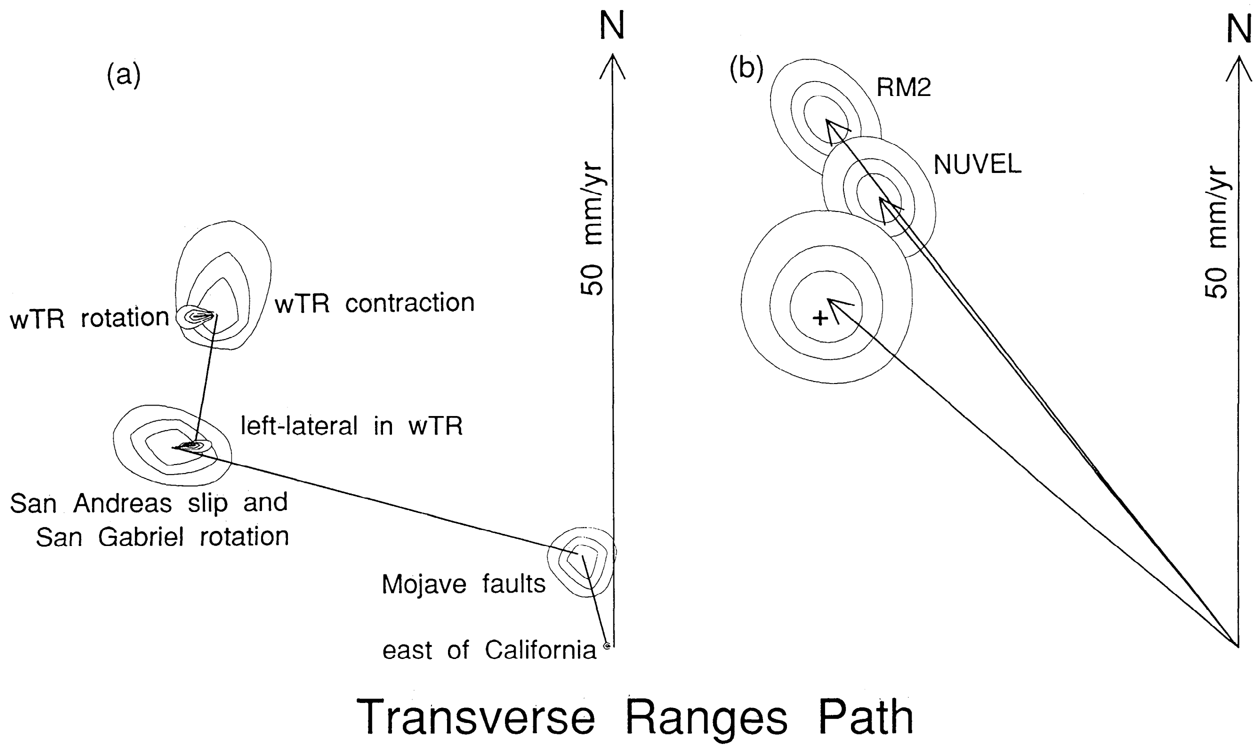

Figure 5. Vector plots for the Transverse Ranges path. Plot is as described in Figure 3. The estimated Pacific-North America velocity is about 11° counterclockwise of the globally based estimates RM2 and NUVEL-1. This results from the nearly westerly velocity contribution of the San Andreas fault for this path, which is not completely compensated for by the northerly orientations of contraction in the western Transverse Ranges (wTR in the figure) and shear across the Mojave faults of the eastern California shear zone.

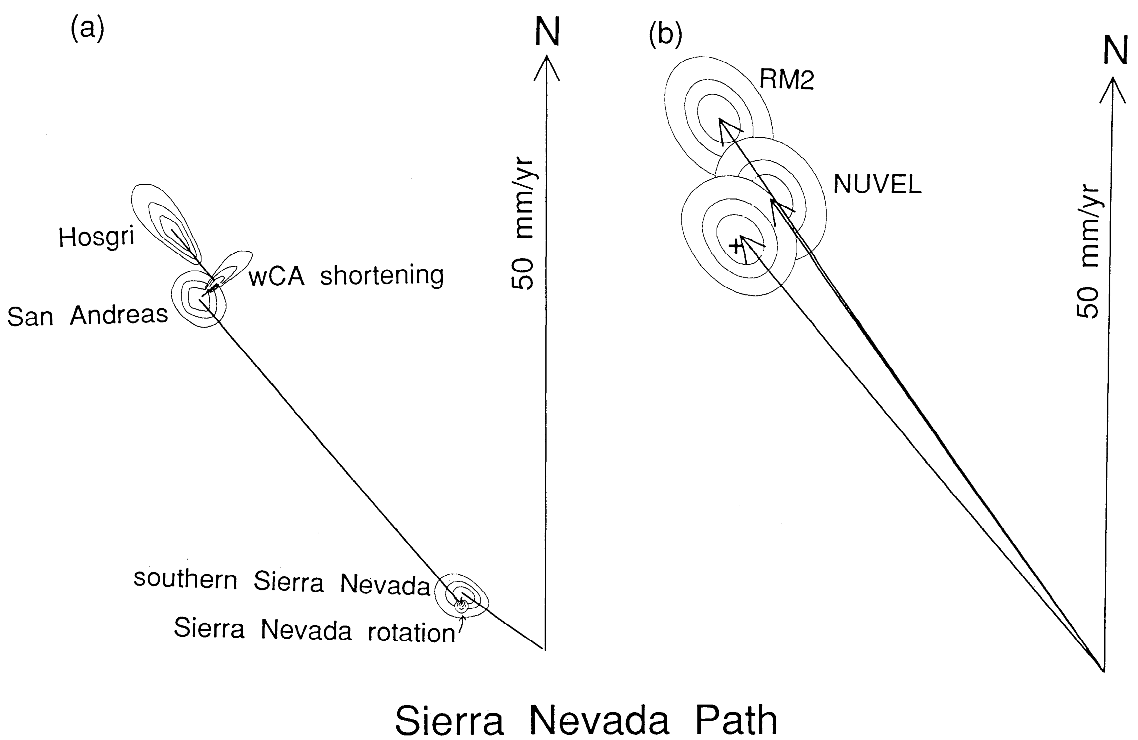

Figure 6. Vector plots for the Sierra Nevada path. Plot is as described in Figure 3. Estimated Pacific-North America velocity is about 5° counterclockwise of the globally based estimates RM2 and NUVEL-1, owing to a slightly counterclockwise orientation of the San Andreas fault in central California and to San Andreas-normal extension rates east of the Sierra Nevada that exceed contraction rates in western California (wCA in the figure). See Figure 7 for "southern Sierra Nevada" velocity estimate.

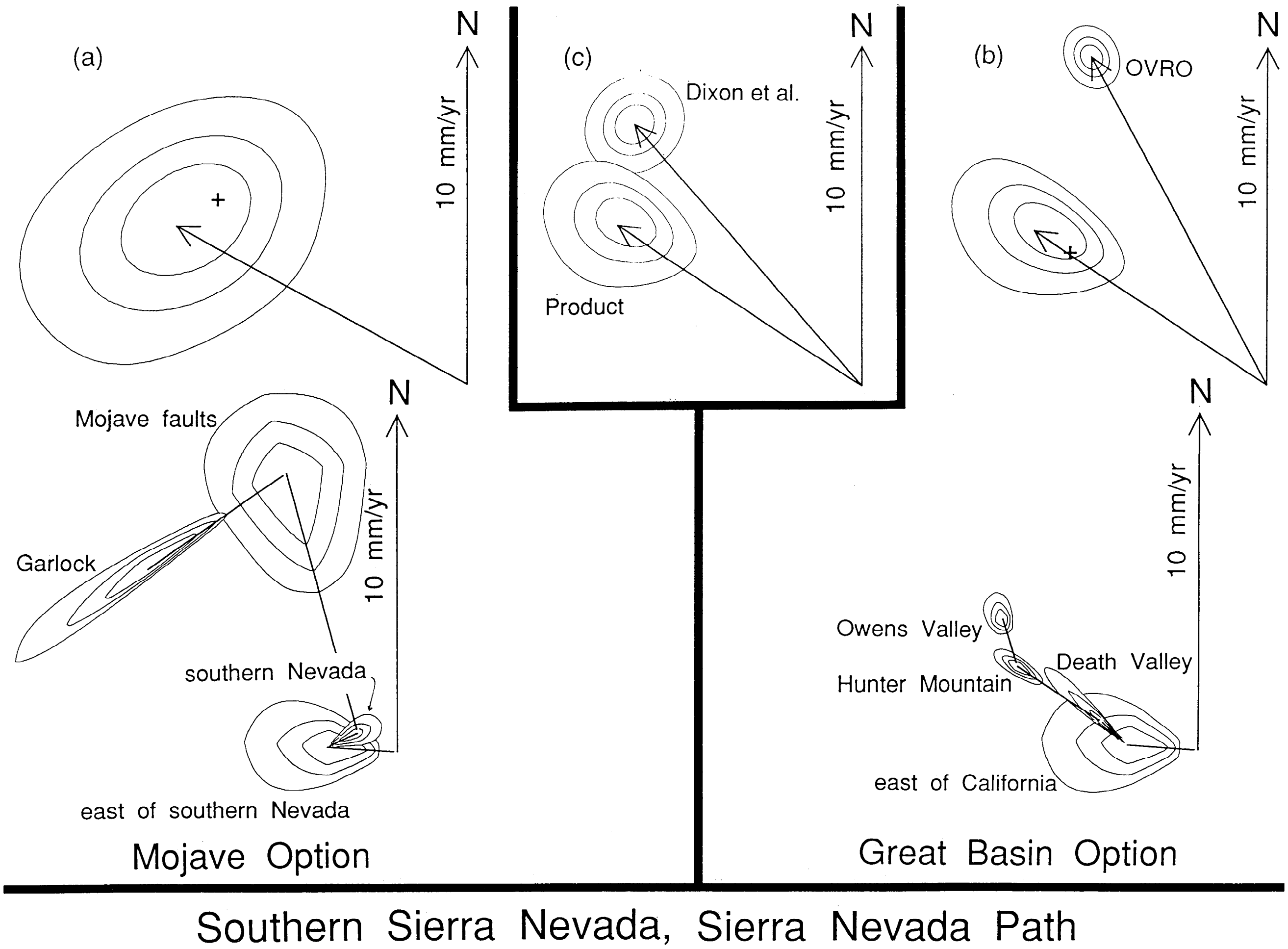

Figure 7. Vector plots for the eastern portion of the Sierra Nevada path. Plot is as described in Figure 3, except scale is expanded (north arrow represents 10 mm/yr). OVRO represents the velocity of a geodetic station in the Owens Valley, near the Sierra Nevada. (a) The velocity data and net convolution results for the Mojave option. (b) The velocity data and net convolution results for the southern Great Basin option. (c) The product of the estimates from Figures 7a and 7b. This is the "southern Sierra Nevada" estimate in Figure 6. The geodetically based velocity estimate for the Sierra Nevada of Dixon et al. (submitted manuscript, 1994) is shown for comparison and discussed in the text.

central California, deformation is organized into three distinctive areas; each area expresses a characteristic pattern of deformation style, and each is represented by one of our paths. The primary goal of this section is to extend the kinematic descriptions beyond the vicinity of the three paths so as to include the southern California region, thereby permitting construction of kinematic models for local regions of interest.

South of the Transverse Ranges

South of the Transverse Ranges, NW trending, right-lateral, strike-slip faults lying to the west of the San Andreas fault account for nearly all of the plate velocity that is not carried on the San Andreas, giving the appearance of a broad simple-shear transform accommodation zone. Faults active in this zone include the subparallel San Jacinto, Elsinore, and southern California continental borderland faults. However, if the crust through which these faults trend is rotating counterclockwise, then the combination of rotation and shear creates a component of pure-shear deformation (as discussed in the last paragraph of this subsection).

If no significant rotation is occurring, activity west of the San Jacinto fault moves the western Peninsular Ranges ~1 cm/yr to the SE with respect to the Pacific plate; slip on the San Jacinto fault adds a similar amount of velocity to the eastern Peninsular Ranges and northern Salton Trough. As shown in Figure 1b, the general trend of these faults, like the San Andreas fault, is ~10° counterclockwise of the NUVEL-1 trend. This produces a Pacific-North America relative velocity estimate that is itself counterclockwise of the NUVEL-1 orientation. Contributing to this more westerly motion is the ~1 mm/yr of extension in the southern Basin and Range. The two VLBI sites lying unambiguously within these blocks that have a well-estimated velocity are located at Monument Peak, about 50 km ENE of San Diego, and Pinyon Flats, east of the San Jacinto fault south of the San Gorgonio Pass (Figure 1b). Their velocities relative to North America [*Ryan et al.*, 1993] are: Monument Peak, 41.5 ±1 mm/yr N52°W ±2°, and Pinyon Flats, 25 ±1 mm/yr N47°W ±2°. These velocities are approximately 10° and 5° counterclockwise of the NUVEL-1 trend (respectively), and consistent with our estimate of motion at these points.

TABLE 2. Predicted Pacific-North America Relative Motion at Selected Points

	End-of-Path Location		RM2		NUVEL-1	
Path	Latitude	Longitude	Rate, mm/yr	Orientation	Rate, mm/yr	Orientation
Sierra Nevada	35.7°	-121.6°	56.9	N35.8°W	48.8	N36.1°W
Transverse Ranges	33.7°	-119.7°	56.8	N38.1°W	48.8	N38.7°W
Peninsular Ranges	32.4°	-118.2°	56.6	N39.7°W	48.6	N40.6°W

Tending to offset the orientation discrepancy between NUVEL-1 and our model for California south of the Transverse Ranges is the velocity contribution arising from a counterclockwise rotation of this crust about the arcuate southern California San Andreas fault. Although the style of this rotation is fairly well defined by the geometry of the bounding faults, the rate is poorly determined. If all of southern California SW of the San Andreas fault rotates at the full rate implied by slip on the San Andreas fault, as suggested by *Weldon and Humphreys* [1986], rotation occurs at ~4°/m.y. As discussed in the appendix, we have chosen a rotation rate for the blocks south of the Transverse Ranges that is half of the full rate (see Figure 4).

The arcuate Agua Blanca fault and continental borderland faults appear to play a role in the rotation of SW California that is the mirror image of the arcuate San Andreas fault in southern California. This is illustrated in Figure 9, which is in a Mojave frame of reference. The almond-shaped pod of crust lying between the San Andreas fault and the Agua Blanca-inner borderland faults rotates counterclockwise so as to avoid converging into the Mojave block, where the San Andreas fault is misaligned with respect to the transform direction. In our model, this pod moves around the curved San Andreas fault and is accommodated at its southern end with slip on the Agua Blanca fault, which separates the rotating pod from the nonrotating Baja peninsula to the south. The pod of crust is also sheared by several northwesterly trending right-lateral strike-slip faults within it. The combination of right-lateral shear in the pod and rotation produces a component of pure shear that allows regional shortening in the north-south direction and lengthening in the east-west direction. Effectively, this contributes to moving most of southern California in a more westerly direction so as to avoid the large left step of the San Andreas fault through the Transverse Ranges.

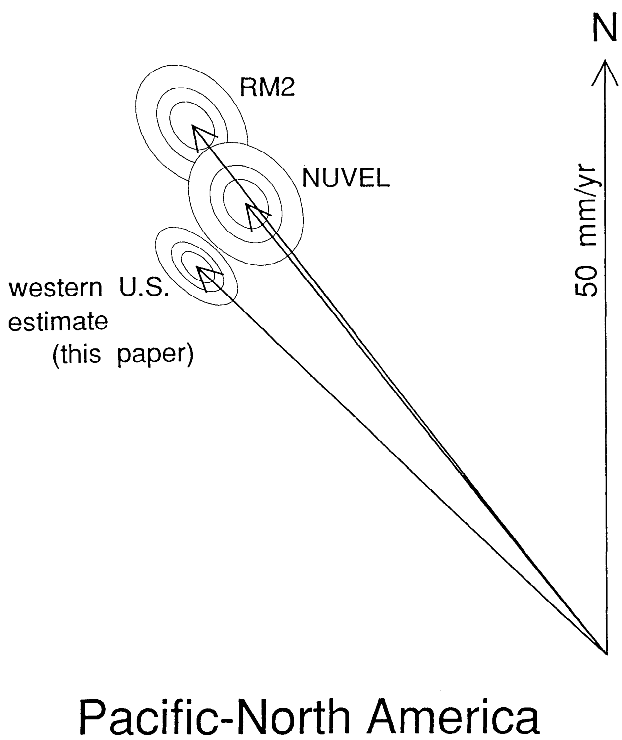

Figure 8. Our final Pacific-North America velocity estimate, compared to Pacific-North America velocity estimates predicted by RM2 [*Minster and Jordan*, 1978] and NUVEL-1 [*DeMets et al.*, 1990]. Plot is as described in Figure 3. Estimated Pacific-North America velocity is about 7° counterclockwise of the globally based estimates of RM2 and NUVEL-1.

Transverse Ranges

Deformation within the Transverse Ranges region is typified by a combination of strike-slip faulting (both right-lateral and left-lateral) and convergence. Both styles are accompanied by block rotations. This activity is largely a consequence of kinematics imposed by the large left step in the San Andreas fault through this region (Figure 1b).

The high eastern San Bernardino Mountains lie north of a relatively small left step in the San Andreas fault through San Gorgonio Pass and are associated with thrusting that has uplifted the San Gorgonio massif and northern platform of the San Bernardino Mountains. This restraining San Andreas fault geometry is local to the San Gorgonio Pass region; the western San Bernardino Mountains have been left standing high from an earlier uplift event (the spectacular southwest escarpment is largely the result of young right-lateral San Andreas faulting juxtaposing high and low regions [*Meisling and Weldon*, 1989]).

The San Gabriel block moves so as to avoid most of the convergence apparently required in this region where the San Andreas fault trends in a strongly restraining direction (i.e., very counterclockwise from its trend elsewhere). However, the broadly arcuate San Andreas fault slips in a strike-slip fashion through this region, which is accomplished by a counterclockwise rotation and relatively great westerly component of velocity of the San Gabriel block (Figure 10a). The crust south of the San Gabriel block is also thought to be involved in the rotation (Figure 9), but at a lower rotation rate than the San Gabriel block itself. Evidence supporting the rotation of California south of the Transverse Ranges include the curved south San Andreas fault [*Weldon and Humphreys*, 1986], the curved Agua Blanca fault (Figure 9 and preceding section), paleomagnetic results in the San Gabriel Mountains (Appendix), and geodetic information (preceding section). Evidence supporting a

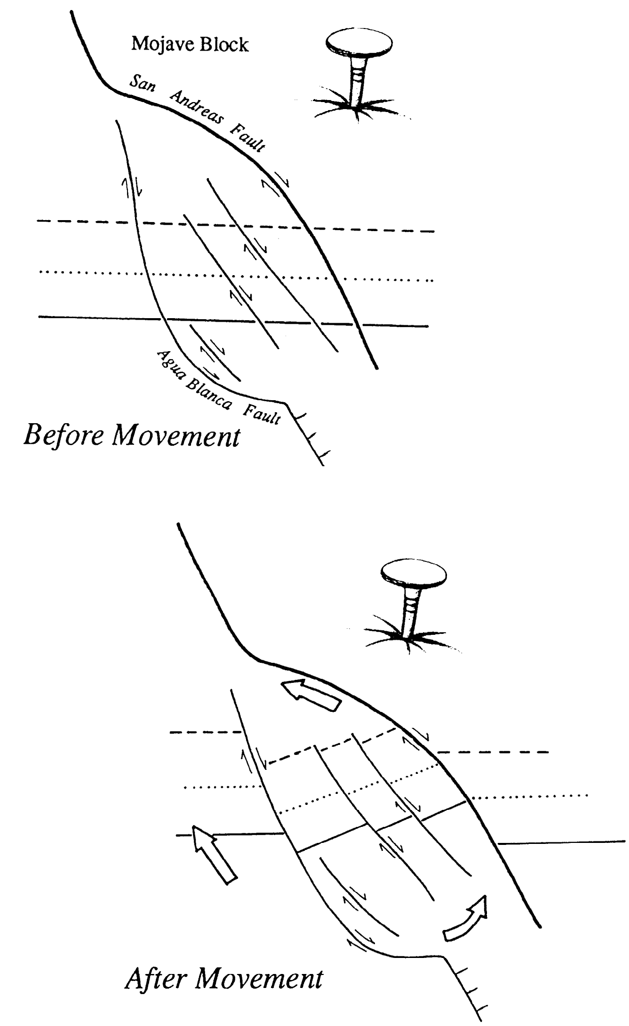

Figure 9. Simplified model illustrating the simultaneous right-lateral shearing and rotation of southern California. With respect to a Mojave reference, this pod rotates counterclockwise about the curved San Andreas and Agua Blanca faults and thus avoids converging into the Mojave block (compare with Figure 1b). The combination of rotation and right-lateral shear within the pod produces a pure-shear style of deformation with N-S shortening and E-W lengthening that accompanies the overall simple shear occurring across the plate margin.

rotation of southern California crust at a rate slower that of the San Gabriel block is found in the left-lateral faulting at the southern margin of the San Gabriel block. If the only important deformation of the California crust south of the San Andreas fault arose from slip on the trans-Peninsula faults (such as the San Jacinto, Elsinore, and borderland faults), then thrusting would occur at increasing rates to the west along the southern margin of the San Gabriel block, as would a component of right-lateral faulting there (see Figure 10b). Such thrusting is observed, but the associated strike-slip faulting is clearly left-lateral. If the San Gabriel block was moving as shown in Figure 10a and the crust to the south was converging towards the Mojave without rotating, as shown in Figure 10b, then strike-slip faulting along the southern margin of the San Gabriel block would be left-lateral. The combination of left-lateral slip on faults south of the San Gabriel block and right-lateral slip on the anomalously trending San Andreas fault to the north result in the San Gabriel block moving more rapidly to the west than any of the surrounding country, like a watermelon seed being displaced to the west between the Mojave and the blocks converging from the south. A consequence of this mechanism is that the San Andreas fault north of the San Gabriel block slips at a rate somewhat greater than one would infer by simply accounting for slip rates on the San Andreas fault and associated faults away from this section of fault. This is supported by the available data [*Weldon et al.*, 1993].

The combined set of observations cited in the preceding paragraph lead us to conclude that the San Gabriel block rotates counterclockwise as it slides along the arcuate San Andreas fault, while the crust south of the San Gabriel block rotates more slowly. This differential rotation between the San Gabriel block and crust to the south, which was not included by *Weldon and Humphreys* [1986], is thought to occur about a pole located near the eastern end of the San Gabriel block because little deformation occurs between the two blocks there.

Deformation in the western Transverse Ranges includes both thrusting and strike-slip faulting, as well as kinematically important rotations. *Luyendyk et al.* [1980] and *Jackson and Molnar* [1990] describe a deformation model for the western Transverse Ranges in which thrusting and left-lateral slip occur on east-west trending faults that separate elongate, clockwise rotating blocks (similar in style to that shown in Figure 11). Alternatively, left-lateral slip on these faults can result from the relatively westerly motion of the western Transverse Ranges with respect to the continental borderland, independent of block rotation. In this latter role, these faults are extensions of the left-lateral faults active at the southern front of the San Gabriel block that allow this block to move west compared to crust to the south. Figure 12 shows both processes being active in western Transverse Ranges, with rotational mechanisms being more active in the westernmost Transverse Ranges and nonrotational shear being dominant near the San Gabriel block.

In the Ventura Basin region in particular, several kinematic processes acting together to produce high rates of shortening (Figure 12). The crust north and east of Ventura Basin rotates counterclockwise due to the motion of the San Gabriel block, while the block south of the Ventura Basin rotates clockwise [*Terres*, 1984; *Terres and Luyendyk*, 1985; *Hornafius*, 1985] about a hinge located near where this block adjoins the San Gabriel block. This activity can be likened to the closing of a folding fan about a pivot located in the vicinity of Los Angeles, with the Ventura Basin and adjoining regions lying between the closing edges of the fan. Also contributing to western Transverse Ranges convergence is the NNW motion of the continental borderland. This component of convergence results from slip on several trans-Peninsular faults (Figure 1b), including the Elsinore fault and faults kinematically related to the Agua Blanca fault, the Rose Canyon and San Clemente faults, which allows the borderland to translate toward the NNW and converge onto the western Transverse Ranges [*Humphreys and Weldon*, 1991].

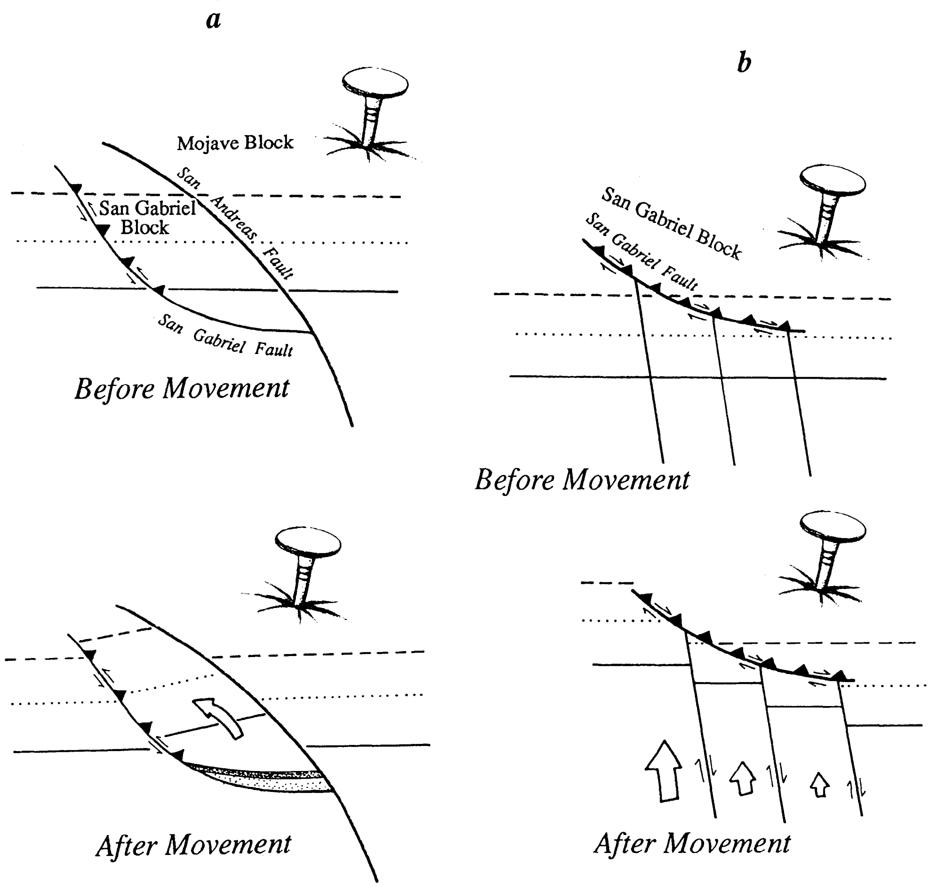

Figure 10. Schematic representations of thrusting mechanisms in the central Transverse Ranges. (a) Illustration showing the San Gabriel block rotating as is moves around the curved San Andreas fault, which is the southern boundary of the fixed Mojave block. Left-lateral faulting occurs near the southern margin of the San Gabriel block. Thrusting accompanies left-lateral faulting to the west. (b) Illustration showing the contribution to Transverse Ranges thrusting provided by right-lateral slip on NNW trending faults lying south of the Transverse Ranges. The rate of convergence increases to the west. The oblique direction of convergence also results in a component right-lateral shear along the range front. This sense of strike-slip motion is different from that predicted in Figure 10a, and is also different from that observed in geologic offset and earthquake slip vectors along the southern margin of the San Gabriel block.

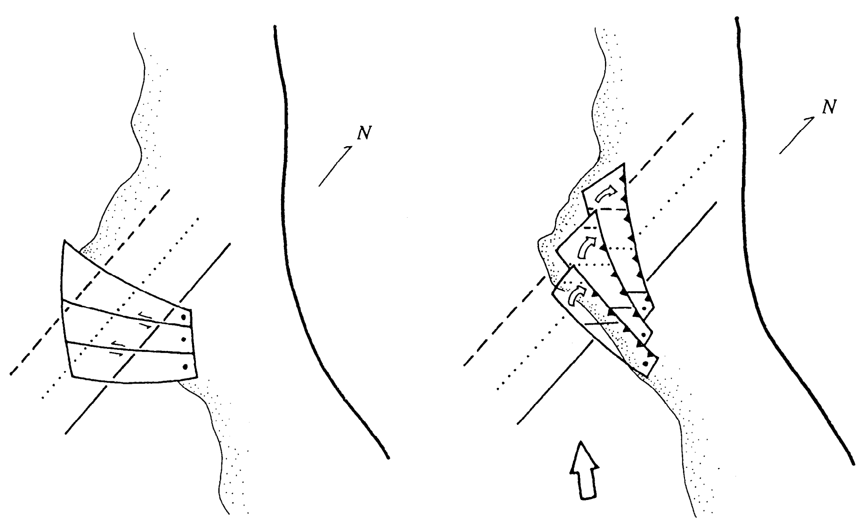

Before Movement *After Movement*

Figure 11. Model where the rotation of elongated blocks create thrusting and left-lateral shear in the western Transverse Ranges. The model is similar to that suggested by *Luyendyk et al.* [1980] and *Jackson and Molnar* [1990], except we show these rotating blocks distributed in a more fan-like pattern. Also unlike Luyendyk et al. and Jackson and Molnar, we do not think that this mechanism applies to regions east of the Ventura Basin, and clearly does not hold for the San Gabriel block.

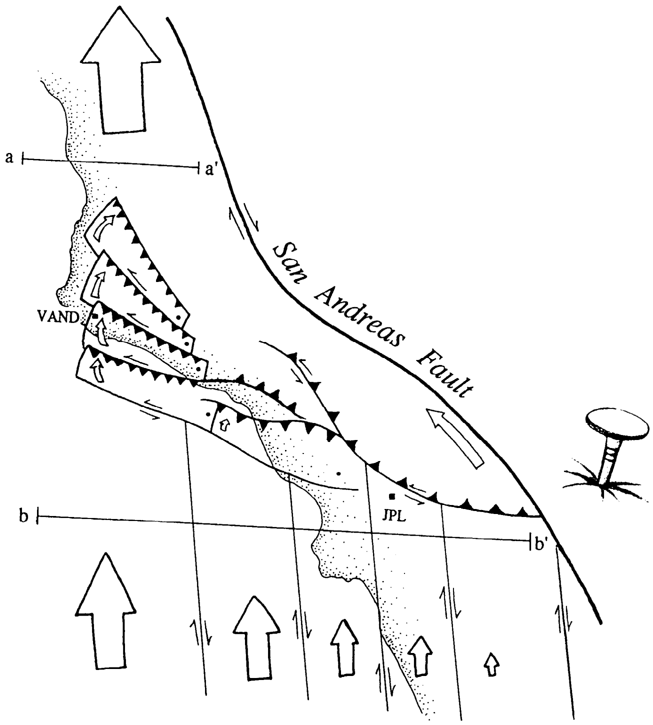

Figure 12. Kinematic model representing current deformation of the western and central Transverse Ranges, using components from Figures 10 and 12. The combined effect of counterclockwise rotation of the San Gabriel block and clockwise rotation of the block south of the Ventura Basin results in rapid convergence across the Ventura Basin, with thrusting on both sides of the basin. West of the Ventura Basin in our model, clockwise rotation of blocks results in thrusting and left-lateral faulting. The lines labeled a-a' and b-b' are used to illustrate the net shortening of crust in an E-W direction that occurs as crust moves northward past the Transverse Ranges. Thrusting in the westernmost Transverse Range results in crustal thickening, whereas clockwise rotation contributes toward an acceleration in velocity and crustal lengthening (both in a San Andreas-parallel direction). Very long baseline interferometry stations VAND and JPL are shown for reference.

The crust of the central and western Transverse Ranges acquires a relatively westerly velocity as a result of its interaction with the relatively west trending San Andreas fault in the Transverse Ranges. As this crust moves into the westernmost Transverse Ranges from the southeast, it rotates clockwise, thereby loosing some of its westerly velocity (Figure 12). In doing so, this crust acquires a velocity nearly parallel to the San Andreas fault north of the big bend. This results is a general "flow" of the crust immediately south of the San Andreas fault that is parallel to the trace of this (sinuous) fault. The funneling of the crust west of the southern California San Andreas fault into the zone west of the central California San Andreas fault (line b-b' to line a-a' in Figure 12) can be accomplished by either (1) a loss of surface area associated with thrusting and crustal thickening or (2) San Andreas-normal shortening and San Andreas-parallel lengthening of the crust as a result of strike slip faulting and block rotation. This second mechanism accelerates the crust of the Coast Ranges toward the NNW (parallel to the San Andreas fault) as crustal blocks of the western Transverse Ranges rotate into the relatively narrow zone of the Coast Ranges.

These two mechanisms trade off with one other, and although both mechanisms appear to be active, the relative importance of crustal thickening and NNW acceleration is not well constrained. Both of these mechanisms have important consequences. In the first mechanism, crustal thickening of the southern Coast Ranges occurs at a relatively great rate as this crust passes the Big Bend of the San Andreas fault. Therefore a significant fraction of the Coast Range shortening that is generally inferred to have occurred normal to the San Andreas fault north of the Big Bend can be attributed to this interaction instead of ongoing rapid convergence in the central California Coast Ranges. In the second mechanism, acceleration of the crust between the San Andreas and Hosgri faults adds to the slip rate of the San Andreas fault and subtracts from the slip rate of the Hosgri fault. The faults of the western Transverse Ranges form a left step in a right-lateral zone of faults found near the southern and central California coast and hence can be considered as a transfer fault [e.g., *Weldon and Humphreys*, 1986]. However, the participating right-lateral faults in central California (principally the Hosgri system) are less active than either the participating right-lateral faults in southern California (between the Elsinore and borderland faults, inclusive) or the transfer faults in the western Transverse Ranges. Crustal acceleration that adds slip to the San Andreas fault and subtracts slip from the Hosgri fault can help decrease this apparent discrepancy.

North of the Transverse Ranges

North of the Transverse Ranges, shear systems nearly parallel to the San Andreas fault are active both east and west of the San Andreas, giving rise to three transform-accommodating shear zones. The eastern system (ECSZ of Figure 1b) splays from the San Andreas fault in the region of the eastern Transverse Ranges, trends through the Mojave [*Sauber*, 1989], and continues on the Death Valley, Panamint Valley, and Owens Valley fault systems [*Dokka and Travis*, 1990; *Powell and Weldon*, 1992], where it is associated with crustal extension in the western Great Basin. (Additional Great Basin extension, oriented approximately E-W, occurs east of the Walker Lane belt.) In contrast, the San Andreas fault and the western fault system (including the Hosgri fault system) are associated with crustal shortening [*Namson and Davis*, 1988; *Mount and Suppe*, 1987; *Feigl et al.*, 1990].

Both right- and left-lateral faults accommodate deformation within the eastern California shear zone (Figure 13), which allows the western Mojave to move NNW with respect to North America at ~1 cm/yr [*Gordon et al.*, 1993]. The right-lateral faults trend northwesterly, and if this orientation alone is used to infer the motion of the western Mojave, the accommodation zone would pull apart. This deformation zone is complex, and local regions of extension and contraction occur where block motions cannot be accommodated simply by strike-slip faults. However, because this zone in the Mojave is neither dilating nor contracting significantly [*Dokka and Travis*, 1990], western Mojave block motion must

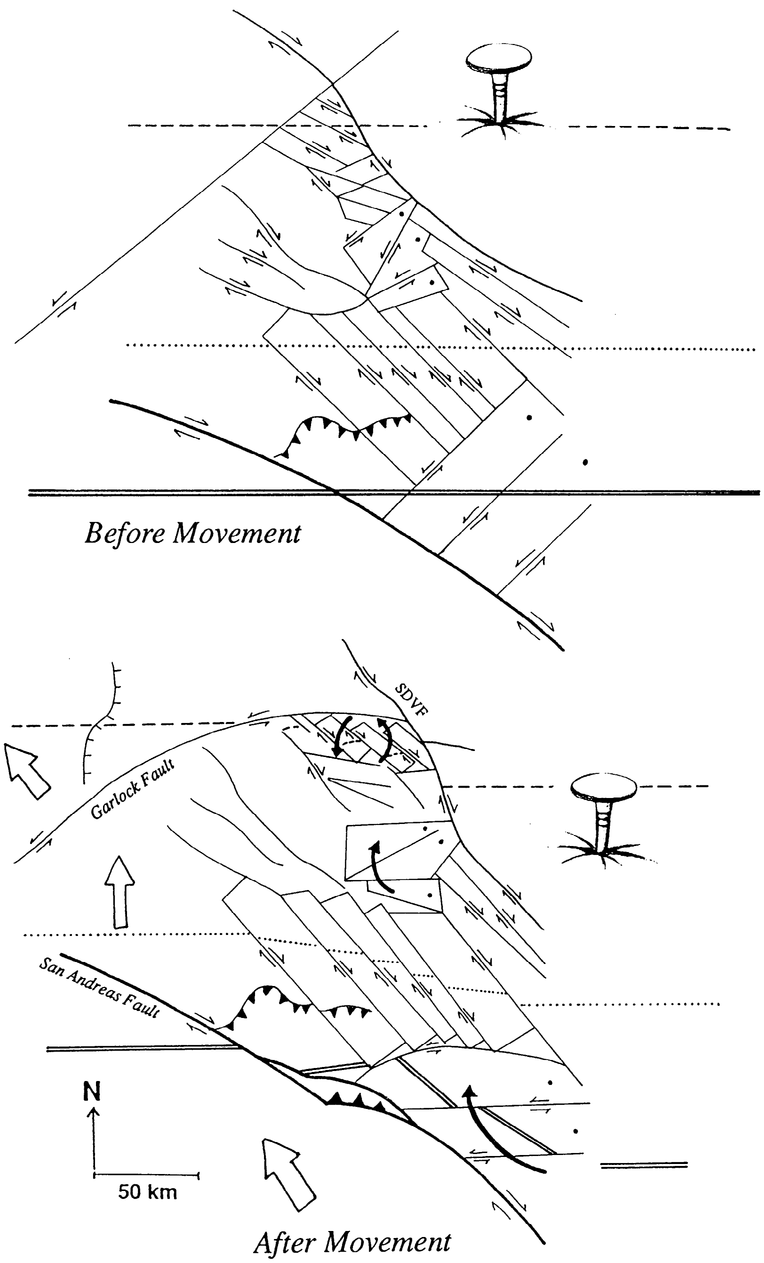

Figure 13. Kinematic model for the motion of the Mojave block relative to eastern California. The Mojave block translates NNW, roughly parallel to the zone of left- and right-lateral faults that accommodate its motion (these numerous faults constitute the eastern California shear zone of Figure 1b). In this model, rotation of the west trending blocks occurs in conjunction with left-lateral slip on the faults that define the blocks (including the eastern Garlock fault). The motion of the Mojave block is more northerly than the right-lateral faults that contribute to its motion, which must be accommodated either by deformation normal to the right-lateral faults or by small amounts of local clockwise block rotation. Slip on the western Garlock fault is not associated with the eastern California shear zone; rather, the left-lateral western Garlock fault separates the northerly moving Mojave block from the northwesterly moving Sierra Nevada block.

approximately parallel the overall NNW trend of this shear zone, and not the trend of individual faults. In our model, the NNW motion of the Mojave block is accommodated by a slight clockwise rotation of the blocks in the central Mojave portion of the shear zone that are bounded by the right-lateral faults. In regions south of the eastern Garlock fault and north and southeast of the eastern Transverse Ranges, a significant clockwise rotation of elongated blocks separated by west trending left-lateral faults [*Luyendyk et al.*, 1985] permits the translation of the Mojave block (Figures 1b and 13). The eastern Garlock fault is included with these faults [*Dokka and Travis*, 1990].

The nearly northerly motion of the Mojave block has two important consequences. First, convergence rates in the Transverse Ranges south of the Mojave are reduced as the Mojave block moves away from the convergent zone (at about 6-8 mm/yr). Second, the northwesterly motion of the Sierra Nevada block and the nearly northerly motion of the Mojave block result in the observed left-lateral slip on the Garlock fault where it separates these two blocks; if the Mojave block were moving northwesterly also, then no strike-slip motion would be resolved on the northeasterly trending Garlock fault there.

North of the Garlock fault (Figure 1b) the style of deformation changes; significant north trending normal faults joined by NW trending strike-slip faults define a set of pull-apart basins that accommodate both right-lateral shear and extension [*Burchfiel et al.*, 1987; *Stewart*, 1988]. Because the trend of this belt aligns with the Mojave zone (ECSZ of Figure 1b) yet is dilating, the Sierra Nevada must be moving away from the average trend of this belt, i.e., moving in a direction more westerly than ~N15°W. We infer that the orientation of right-lateral faults (~N50°W) represents the orientation of relative motion across the zone as a whole, resulting in a creation of surface area. T. H. Dixon et al. (Constraints on present-day Basin and Range deformation from space geodesy, submitted to *Tectonics*, 1994; hereinafter referred to as Dixon et al., submitted manuscript, 1994) discuss the occurrence of additional Great Basin extension, directed roughly eastward, occurring at significant rates east of the Walker Lane belt. It is this extension, combined with a near absence of southern Basin and Range extension, that results in a Sierra Nevada motion that is more westerly than the Mojave block. The left-lateral western Garlock fault accommodates this difference in relative motion in a manner similar to that proposed by *Davis and Burchfiel* [1973]. In our model, eastern Garlock fault activity is due both to its role in separating clockwise rotating blocks in the Mojave and to its role in accommodating a component of Garlock-parallel extension to its north; the western Garlock fault is active only in the latter role, and is presumably less active. The northward continuation of the eastern California shear zone includes the Walker Lane belt [*Stewart*, 1988] and several deformation zones trending through the Pacific Northwest [*Pezzopane and Weldon*, 1993].

Discussion

Pacific–North America Relative Motion

Our estimate of Pacific-North America relative motion (Figure 8) is calculated using data associated with the deformation zone in the southwestern United States that accommodates the relative motion, and it is independent of other estimates of plate motion. In this sense it is complementary to the models NUVEL-1 [*DeMets et al.*, 1990], NUVEL-1A (DeMets et al., submitted manuscript, 1994), and RM2 [*Minster and Jordan*, 1978], which are derived from plate kinematic information that is exclusive of data from our study area. Our locally based rate estimate is not significantly different from that of NUVEL-1 or NUVEL-1A (and is about a centimeter per year slower than the older RM2 rate). Thus our rate estimate is consistent with the rate given by the global data set. However, our locally based orientation estimate is ~7° more westerly than the globally based estimates (Table 1).

Several possible explanations for this discrepancy are listed below, and some combination of these factors probably explains the difference in orientation. (1) There is a small chance (less than 1%) that the models are consistent within their probability distributions as described. In order for the models to be consistent, velocities for individual features in the western United States must be chosen toward the northeast limits of their respective probability fields, whereas velocities for individual features in the NUVEL-1 model must be chosen so as to result in a Pacific plate motion that is biased toward a southwest orientation. If the two models are consistent, then the kinematic solution for the southwest United States is very well constrained by the product of these two velocity probability distributions. (2) The NUVEL-1 velocity estimate for Pacific-North America motion does not represent the southwestern United States properly because deformation of the Pacific plate occurs somewhere between the southwest United States and the regions where kinematic constraints on Pacific plate motion exist. (3) There is significant deformation in the southwest United States that we have not included in our model. The possibility of unaccounted for deformation results in end-of-path error estimates that are too small. However, we have been careful to include all significant deformation of which we are aware, and we consider it unlikely that significant deformation has gone unrecognized. The fact that our rate estimates are very similar to the NUVEL-1 rate supports the contention that important deformation has not been omitted, especially because most deformation contributes a component that adds to the Pacific-North America rate. The velocity fields that we would most likely fail to recognize are those associated with rotations. (4) Significant deformation occurs in the region west of our model (such as shortening near the continental rise), and hence we have not integrated deformation all the way to the Pacific plate. If this were the sole cause of the discrepancy, about 6 mm/yr of oblique contraction would be required offshore. Such contraction seems unlikely considering the structural simplicity of young sediments and the relative seismic quiescence of this region.

Nonideal Transform Deformation

The Pacific-North America transform deformation field differs from its oceanic counterparts in two important ways. First, transform-related deformation is broadly distributed, extending across California and portions of westernmost Nevada. Second, significant amounts of deformation involve either the creation or the destruction of surface area. This sometimes occurs where fault patterns are complex and local space problems exist. However, we also find large regions that experience a gain or loss of surface area. Figure 14 shows an interior belt of dilation and a western belt of contraction, each occurring within the zone of transform accommodation. The dilating belt extends across the entire region studied except through the Mojave. The belt of contraction includes the Coast Ranges and the Transverse Ranges. A southward continuation of the contractional belt within the southern California continental borderland is

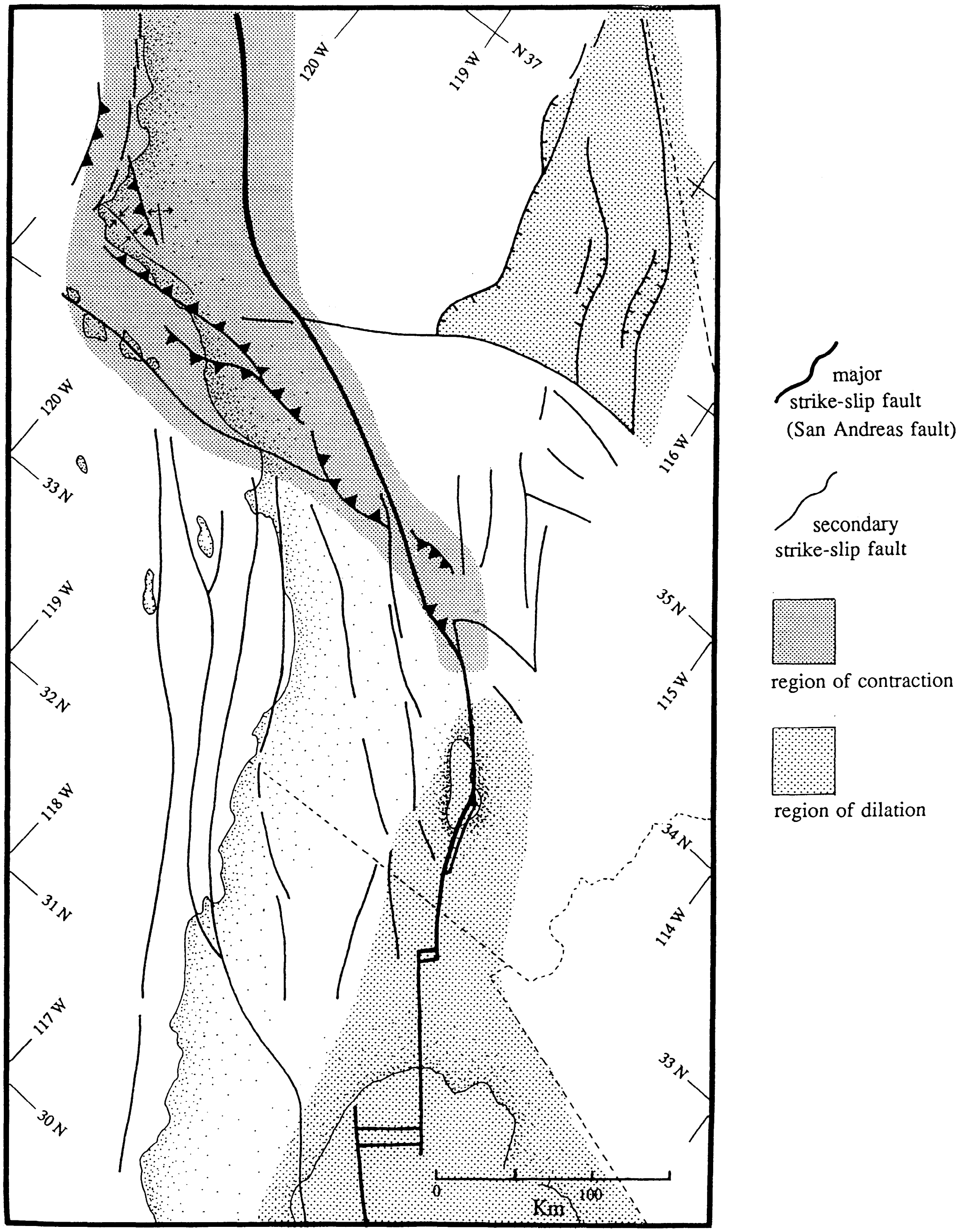

Figure 14. Schematic regional map emphasizing regions of positive and negative dilation that are associated with important shear zones. Surface area is being created in the Salton Trough region and the region of the SW Great Basin, both shown with stipples. Surface area is being lost in the central California Coast Ranges, the Transverse Ranges. and perhaps in the northern borderland, shown with ruled pattern. See Figure 1b for names and locations of structural features.

suggested by the occurrence of borderland earthquakes showing thrust components [*Legg*, 1988; *Pacheco and Nabelek*, 1988; *Hauksson and Jones*, 1988] and by young folds and thrusts [*Mills and Fischer*, 1991]. The San Andreas fault zone is associated with the Gulf of California and the Coast Ranges regions of positive and negative dilation, respectively. In both settings, the San Andreas fault is oriented counterclockwise of the NUVEL-predicted Pacific-North America relative position vector and essentially parallel to our estimate of this vector. The transition between the dilational and contractional San Andreas domains occurs near the eastern Transverse Ranges.

Deformation in the western Great Basin and the California Coast Ranges involving positive and negative surface dilation (respectively) defines paired tectonic belts. The western Great Basin has active normal faults oriented nearly parallel to the Pacific-North America relative motion vector (e.g., the frontal faults of the Sierra Nevada), and the dominant strike-slip faulting there is oriented so as to move the Sierra Nevada/Great Valley block toward the Pacific (see Figure 7b). At the same latitude, contraction occurs in the central California Coast Ranges [e.g., *Mount and Suppe*, 1987] that is oriented at a high angle to the Pacific-North America relative motion vector (see Figure 6). Together, these zones of deformation give rise to a transform-normal component of motion to the Sierra Nevada/Great Valley block. This suggests the action of forces created locally that are not directly attributable to transform deformation [e.g., *Eaton*, 1932].

Another region where deformation occurs that is not related simply to transform faulting is the Transverse Ranges. Geodynamic modeling of this region indicates that locally generated forces, attributed to anomalously dense mantle sinking beneath the Transverse Ranges, drive crust toward the Transverse Ranges [*Bird and Baumgardner*, 1984; *Sheffels and McNutt*, 1986, 1987; *Humphreys and Hager*, 1990]. Because actual rates of shortening across most of the Transverse Ranges are relatively slow (i.e., <5 mm/yr), approximate force balance appears to exist between convergence-driving forces created in the mantle and divergence-driving forces created by the high topography [*Humphreys and Hager*, 1990]. In contrast, shortening rates in the western Transverse Ranges probably exceed 10 mm/yr. This loss of surface area occurs primarily west of the Big Bend, i.e., in the western Transverse Ranges, presumably because the lithosphere of the western Transverse Ranges is relatively weak compared to that of the Great Valley (supported by upper mantle images [*Biasi and Humphreys*, 1992; *Humphreys and Dueker*, 1994]), and because the crust in the western Transverse Ranges is being drawn toward a zone of mantle downwelling beneath at least part of this region [*Humphreys and Hager*, 1990].

Styles of deformation are distinctive within the areas of nonideal transform accommodation. Surface area dilation tends to occur within pull-apart steps of major right-lateral strike-slip systems. The associated normal faults are incorporated directly into the fault system and trend obliquely to the orientation of the strike-slip elements (see Figure 15). The Salton Trough has been attributed to this style of kinematics [e.g., *Elders et al.*, 1972], as have the California valleys east of the southern Sierra Nevada (as discussed above). In both regions, large amounts of crustal extension have occurred on fault systems that contribute nearly directly toward transform shear accommodation (although, at least in the region east of the southern Sierra Nevada, some extension occurs on faults that contribute motion that is at a high angle to the strike-slip system). In contrast to the kinematics of transtension, transpression typically is accommodated with folds and thrust faults that lie off of the dominant local shear system and allow contraction in a direction that is nearly normal to this system. This style is described above for the Transverse Ranges and is well expressed in the Coast Ranges [e.g., *Mount and Suppe*, 1987] and has been proposed for the southern Los Angeles basin [*Hauksson and Saldivar*, 1989].

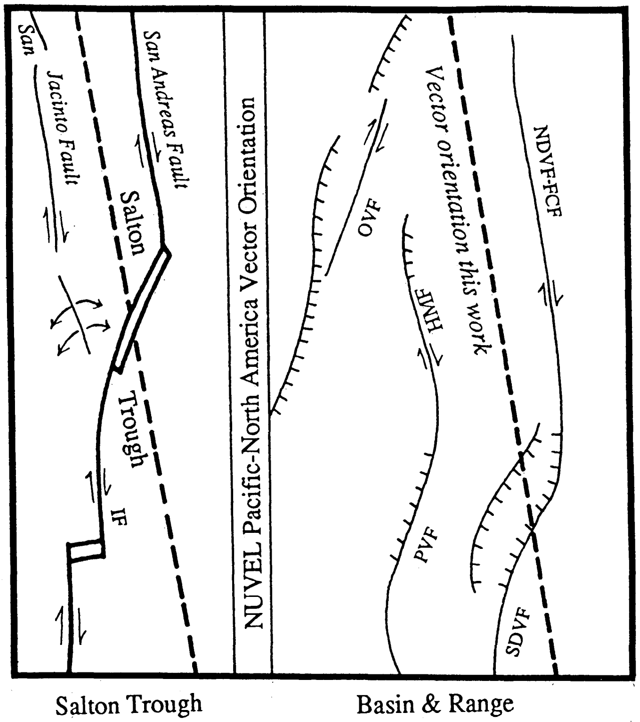

Figure 15. Examples of the styles of deformation where extensional features are incorporated into the strike-slip fault structures. For reference, lines parallel to the Pacific-North America velocity estimates from from NUVEL-1 (sides of figure) [*DeMets et al.*, 1990] and our work (dashed lines) are shown. If shear were applied across the region of transtension, the NUVEL-1 orientation would cause compression normal to the most of the strike-slip faults, whereas these faults are well aligned for simple shear with respect to the dashed line. Zone of folding accommodating shortening is shown with double-sided arrows. See Figure 1b for names and locations of structural features.

Conclusions

We estimate Pacific-North America relative motion by integrating deformation along three paths across the SW United States from east of the Rio Grande Rift to near the continental escarpment, thereby crossing the deformation field accommodating relative transform motion. The kinematic information from each path is nearly independent of that from the other paths, providing independent estimates of the Pacific-North America relative velocity. These estimates are consistent with each other and combine to produce a Pacific velocity estimate of 48 ±3 mm/yr N45°W ±2° with respect to North America (for a location south of the western Transverse Ranges). Most of the kinematic information used in our study is based upon deformation representing average rates younger than 20,000 years. The global models NUVEL-1 [*DeMets et al.*, 1990] and NUVEL-1A (DeMets et al., submitted manuscript, 1994) also strive for an estimate of ongoing motion (by using magnetic lineation data younger than about 3 m.y.). Compared to the velocity predicted by NUVEL-1 and NUVEL-1A, our estimate is similar in rate but our direction for the Pacific plate relative velocity is more counterclockwise (i.e., westerly) by 7° ±2°. The strongest orientation constraint is obtained from the southern path, where the deformation occurs primarily on strike-slip faults that trend ~10° more counterclockwise in orientation that of the NUVEL-1 trend. Deformation on the other minor features encountered along this path does not change this orientation significantly.

The kinematic information used in our velocity calculations for the three paths represent three distinct regions, each expressing a different style of transform deformation. The northern region (central California) and southern region (southern California), which accommodate transform motion with relatively simple deformation fields, are kinematically joined across the complex Transverse Ranges region. Loosely defined, two important shear zones are active: one near the continental margin and another near eastern California. The zone near the margin includes the San Andreas and Hosgri systems in the northern region and borderland and trans-Peninsular faults in the southern region. The eastern zone includes the San Andreas in the southern region and the shear zones in the Mojave and the western Great Basin. Throughout this entire area the San Andreas fault is the dominate structure. However, its rate varies from region to region as it interacts with the two lesser transform-accommodating shear zones. Both of these shear systems splay from the San Andreas in the vicinity of the Transverse Ranges (Figure 1b), with the trans-Peninsular system trending SSE from the western and central Transverse Ranges and the eastern California shear zone trending NNW from the eastern Transverse Ranges.

Secondary faulting near the San Andreas fault also varies from region to region, accommodating dilation in the southern region and contraction in the northern region. The San Andreas fault defines a large left step where it passes through the Transverse Ranges, which would appear to require high rates of convergence in this region; however, southern California crust moves so as to experience only relatively minor rates of convergence there. This is accomplished by a combination of the movement of the Mojave block to the north and away from the zone of convergence (Figure 13) and by a counterclockwise rotation of the crust south of the Transverse Ranges as it moves around the arcuate San Andreas fault (Figures 9 and 10a), causing a reduction of its northern velocity (and an increase in its western velocity). Crust in the western Transverse Ranges shortens and rotates clockwise to flow in a NNW direction, nearly parallel to the San Andreas fault in central California. The counterclockwise and then clockwise rotations of southern California crust, in conjunction with increasing amounts of crustal contraction, result in a "funneling" of crust south of the Transverse Ranges into the relatively narrow central California Coast Ranges to the north (Figure 12).

Appendix: Detailed Description of Deformation Encountered Along the Three Paths

In this appendix we present and discuss the kinematic information used to infer the pattern of deformation in the southwest United States and the Pacific-North America relative motion that it accommodates. Values used in Table 1 are indicated below with daggers. The Transverse Ranges path is discussed first because it is our reference path and because the Rio Grande Rift is most easily introduced for this path. A disproportionate amount of the following discussion focuses on the low deformation rates occurring across the western United States east of California. Although these rates are relatively inconsequential, it is important to demonstrate that they do not accommodate the difference between the globally estimated Pacific plate velocity and the local Pacific plate velocity estimated below. In fact, deformation east of California tends to increase this discrepancy.

Transverse Ranges Path

Rio Grande Rift. The first significant deformation encountered along the Transverse Ranges path is the Rio Grande Rift (Figure 1a), a series of basins bounded principally by normal faults, which extends ~1000 km from the Mexican border to northern Colorado [*Chapin*, 1979; *Kelley*, 1979]. The rift has been associated with extension of the greater Basin and Range region [e.g., *Stewart*, 1978; *Tweto*, 1979]. Also, because deformation across the rift is the only significant deformation occurring between North America and the Colorado Plateau, modern motion of the Plateau has been kinematically related to deformation within the rift. Most workers agree that extension across the rift increases to the south [e.g., *Chapin*, 1979] in a manner consistent with rotation of the Colorado Plateau about a pole located near the northern termination of the rift [*Kelley*, 1979; *Golombek et al.*, 1983]. Away from the central rift, which trends 15° more easterly than the overall rift, major faults within the rift as well as the rift itself trend north. Within the central rift, both structural [*Kelley*, 1979] and paleomagnetic data [*Golombek et al.*, 1983] indicate extensional faulting with a component of left-lateral slip. Left-lateral deformation could result from rotation of the plateau or simple west directed extension across the relatively easterly trending central rift. In light of the style of deformation north and south of the central rift, the second option appears more likely. Therefore we assume that extension occurs N90°W †, perpendicular to this trend. Because rifts commonly open in directions oblique to their trend we assign an uncertainty in orientation of ±30° †, which is greater than the variations in trend of the major faults within the rift. We choose 30° because this is the range in extension direction that may occur on oblique normal faults without the accompaniment of significant amounts of strike-slip faulting [*Withjack and Jamison*, 1986]. Our uncertainty range admits the possibility that strike-slip faulting related to Colorado Plateau rotation occurs at about half the extension rate.

The long-term average extension rate across the central rift has been ~0.2 mm/yr, and the late Quaternary rate is inferred to be ~0.14 mm/yr [*Golombek*, 1981; *Golombek et al.*, 1983]. We use the Quaternary extension rate of 0.14 † mm/yr as the most likely rate for the central rift. For the upper limit we use the long-term average of 0.20 † mm/yr, and for the lower limit we arbitrarily choose 0.10 † mm/yr. There are no published data for the relative magnitude of left-lateral shear, but it is inferred to occur at a fraction of the extension rate.

Colorado Plateau rotation. The kinematics of Colorado Plateau rotation can be described with an Euler pole. We estimate this pole position with information on Rio Grande rifting, assuming that both North America to the east of the rift and the Colorado Plateau are rigid entities. Above, we used a N90°W direction and an extension rate diminishing to zero at the Colorado-Wyoming border, which define our preferred pole position. The kinematic implications of rotation about this pole are consistent with mild north directed shortening along the northern Colorado Plateau margin [*Hamilton*, 1988a]. The previously assigned rifting orientation uncertainty of ±30° corresponds to a pole position uncertainty in longitude of ±300 km. This range in possible pole position does not conflict with the style of deformation observed within several hundred kilometers east and west of the northern rift, which is not noted as being significantly active. Thus our best estimate of the pole position is at the intersection of the Wyoming-Colorado border with the Rio Grande trend (this coincides with the best estimate of *Golombek et al.* [1983]), and we use an uncertainty in the pole position of 300 km to describe the uncertainty in plateau motion and rift opening.

The Colorado Plateau-North America pole position, together with the extension rate of 0.10–0.20 mm/yr across the central Rio Grande Rift that we discussed above, imply a plateau rotation rate of 0.01–0.02°/m.y. Considering the uncertainty in pole position, and because either the Colorado Plateau or Wyoming may not be behaving exactly as we have assumed, we widen these limits to 0.0–0.04°/m.y. The domain of possible pole positions and the NNW trend of the central Rio Grande Rift imply a ratio of left-lateral rate to rift rate of between 0.00 and 0.7, with a best estimate of 0.25.

Paleomagnetic data also supply information on Colorado Plateau rotation. *Steiner* [1986] documents 9–14° of net clockwise rotation about a Colorado Plateau-North America Euler pole near the SW margin of the plateau. However, Steiner suggests that there have been three episodes of rotation, with the Cenozoic being the least important, and that the SW plateau pole position is most consistent with pre-Cenozoic rotation. This interpretation is consistent with Laramide-age deformation east of the Colorado Plateau that may have accommodated plateau rotation during this time [*Hamilton*, 1988a, 1988b; *Greis*, 1983]. Thus we interpret the paleomagnetic data to be consistent with the late Cenozoic geologic data, but of lower resolution. We therefore use the geologically inferred deformation of the Rio Grande Rift to describe the rotation of the Colorado Plateau.

The Transverse Ranges path continues ~600 km across the Colorado Plateau. At the western margin of the plateau, the inferred plateau rotation rate results in a velocity vector (relative to North America) of 0.1† ±0.1† mm/yr oriented north† ±30°†. The net velocity vector at this point, which is the sum of Rio Grande extension and Colorado Plateau rotation, is 0.25 mm/yr (oriented roughly in the Pacific Plate-North America relative direction). Compared to deformation rates found to the west, this vector is negligible.

Basin and Range. Our path leaves the SW Colorado Plateau and crosses a portion of the Basin and Range in NE Arizona and southernmost Nevada. The most significant deformation encountered along this portion of the path occurs on a family of predominantly normal faults near the western margin of the Colorado Plateau. Faults strike essentially north where our path crosses this system, suggesting a westward† extension direction. As above, we assign ±30°† from this direction to permit oblique extension. The northern continuations of these faults have been studied in SW Utah [*Hamblin et al.*, 1981; *Mayer*, 1986], the most active of these being the Hurricane fault. From this work we infer a rate of about 1.0 mm/yr for the entire zone bounding the western Colorado Plateau. As discussed below in the section on the Sierra Nevada path, geodetic information suggests that the Great Basin extension rate may be underestimated. However, the southern continuations of the plateau-bounding faults appear less active than they are in SW Utah, which is consistent with the occurrence of left-lateral strike-slip activity on the WSW trending Lake Mead fault system [*Bohannon*, 1979, 1984], a set of faults that lie between the Colorado Plateau-bounding faults in Utah and those in NW Arizona (Figure 1a). We choose a rate of 0.5† ±0.5† mm/yr to represent the deformation rate of the plateau-bounding faults where traversed by our path. This range allows the boundary of the plateau south of the Lake Mead system to be completely inactive or to extend at a rate equal to the estimated extension rate in SW Utah. The net velocity at this point is a relatively small 0.6 ±0.5 mm/yr N81°W ±35° (Figure 5).

Mojave faults. Very little deformation is encountered in the Mojave Desert east of longitude 116°W. West of longitude 116°W is an active set of faults that define a NNW trending shear zone separating the Mojave block from crust to the east that moves nearly with North America [*Dokka and Travis*, 1990]. This eastern California shear zone is composed of NW striking right-lateral faults, east trending left-lateral faults, and less significant dip-slip faults of diverse trends. The average strike of the most active right-lateral faults is N41°W, with deviations of ±10°. This orientation is considerably more westerly than the trend of the zone as a whole, so that if the orientation of the right-lateral faults alone is used to infer Mojave motion, the accommodation zone would pull apart. Because this zone is neither dilating nor contracting greatly [*Dokka and Travis*, 1990], Mojave block motion must approximately parallel the average trend of this shear zone, and the blocks bounded by the right-lateral faults must rotate clockwise slightly to accommodate the motion of the Mojave. This is consistent with geologic [*Dokka and Travis*, 1990] and paleomagnetic data [*Wells and Hillhouse*, 1989] for the region. We estimate that the overall shear zone has an orientation of about N15°W†.

Our best orientation estimate assumes that the shear zone accommodates western Mojave motion without involving net extension or contraction within the zone. However, the faults within the shear zone bound a series of valleys that may accommodate a component of normal faulting. We infer that the valleys are attributed to either local right stepping of strike-slip motion or the formation of rhombochasms where conjugate left-lateral and right-lateral faults meet. Shortening (such as that reported by *Bartley et al.* [1990]) is similarly attributed to local fault geometry. We choose an uncertainty in the orientation estimate that is wide enough to encompass a range of possibilities that include simple strike-slip faulting on the dominant right-lateral faults in the Mojave [*Sauber et al.*, 1986] and the possibility that contraction [*Bartley et al.*, 1990] and modest crustal thickening occurs because the western Mojave block moves in a direction that is more northerly than the average trend of the shear zone. This range of possibilities is bounded by $\pm25°^{\dagger}$.

Dokka and Travis [1990] estimate a net late Cenozoic offset of 65 km across these faults, with deformation initiating between ~10 and 6 Ma. They report that deformation has shifted recently from the eastern to the central set of Mojave faults. Net late Cenozoic offset across the mid-Mojave fault zone is about 35 km [*Dibblee*, 1967; *Powell*, 1981; *Dokka*, 1983]. If western Mojave faulting became active with the initiation of the modern San Andreas fault activity ~5 Ma, a rate of 7 mm/yr is implied (though no strong evidence exists for the time of slip initiation on these faults). A similar rate is obtained by averaging the net ~65 km of offset over 10 m.y. Geodetic data yield similar results. Land-based data [*Savage et al.*, 1990] suggest that this shear zone trends about N35°W and accommodates ~8 mm/yr of simple right-lateral shear. The VLBI station "Mojave" in the northern Mojave moves with respect to North America at 9 mm/yr N20°W [*Ward*, 1990], with a negligible formal uncertainty in its site velocity.

We represent activity on the Mojave portion of the eastern California shear zone with a vector of $8^{\dagger}$ mm/yr N15°W† and uncertainties of +3-4† mm/yr and $\pm25°^{\dagger}$. This rate is slightly greater than the ~7 mm/yr estimated geologically across the right-lateral faults so as to include a contribution from the conjugate faulting, and the uncertainty limits encompass the range in rate estimates. The uncertainty assigned to this deformation is relatively great because we are not sure how the geodetic rate compares with the geologic rate, and the geologic rate, while consistent, is poorly constrained. The upper limit allows the geologically estimated offset of 65 km to occur at rates slightly faster than average over the shortest interval allowed, i.e., since 6 Ma [*Dokka and Travis*, 1990]. The lower limit allows 45 km of net offset (our estimate of the minimum net offset, based on the work of *Dokka and Travis* [1990]) to have occurred steadily since 10.6 Ma (the maximum duration considered possible by *Dokka and Travis* [1990]).

There has been considerable debate on the subject of late Cenozoic block rotations within the Mojave. Large-scale counterclockwise [e.g., *Garfunkel*, 1974; *Calderone and Butler*, 1984] and clockwise [e.g., *Luyendyk et al.*, 1980; *Bird and Rosenstock*, 1984] rotations have been proposed. More recent paleomagnetic work in the southern [*Weldon et al.*, 1984; *Winston*, 1985; *Weldon*, 1986], central [*Wells and Hillhouse*, 1989], and southeastern Mojave [*Calderone et al.*, 1986; 1990] suggest that except within fault zones the Mojave has rotated less than 5° since the late Miocene. In particular, the zones in which *Luyendyk et al.* [1980] proposed clockwise rotation lie within the eastern California shear zone. Also, the lack of an eastern structure to form a rotational boundary for the Mojave block argues against significant rotation of the Mojave as a whole. Our assigned uncertainty in orientation will accommodate Mojave block rotation at rates of ±1°/m.y.; we consider rotation rates beyond this range as unlikely.

San Andreas fault. The path next crosses the San Andreas fault at a location where agreement exists between the short-term and long-term slip rates. *Weldon* [1986] proposed a slip rate of 37.5 ±2 mm/yr based on offset of early to middle Pleistocene fanglomerates, dated by volcanic ash beds and paleomagnetic information. A more conservative reevaluation of an expanded data set [*Weldon et al.*, 1993] concludes a rate of 36 ±8 mm/yr. This rate has been confirmed for slip during the past several hundred years (36 ±7 mm/yr [*Salyards*, 1988; *Salyards et al.*, 1992]) as well as for the past 4-5 m.y. (~35 mm/yr [*Matti et al.*, 1985; *Frizzell et al.*, 1986; *Weldon*, 1986; *Meisling and Weldon*, 1989]), and we use this more conservative value as our rate estimate. Also, this rate is consistent with the summed rates of the San Andreas and San Jacinto faults to the south, as proposed by *Weldon and Sieh* [1985]. Despite this evidence, there are workers who believe the slip rate is either greater or less: rates as low as 20 mm/yr [*Barrows et al.*, 1985] and 20-38 mm/yr [*Schwartz and Weldon*, 1986] have been proposed, and rates of greater than 50 mm/yr have been proposed by *Rust* [1982] and *Ramirez* [1982]. Geodetic measurements suggest San Andreas rates near 30 mm/yr. Space-based geodetic results suggest 26.9 ±2.6 mm/yr [*Sauber*, 1989], while land-based results have been interpreted to yield far-field rates of 18.3 ±1.2 [*Prescott et al.*, 1987], 30 ±6 [*Eberhart-Phillips et al.*, 1990], and ~36 mm/yr [*Savage*, 1990]. The differences in geodetically estimated rate reflect, primarily, differences in the parameterization of the deformation model used in fitting the data. All of the above San Andreas rate estimates that deviate by more than a few millimeters per year from 36 mm/yr are based either on geodetics (that also can be interpreted at rates of ~36 mm/yr) or on the offset of poorly defined or dated features. Because the more recent interpretations of the geodetic data are consistent with the relatively well constrained geologic estimates, we consider the lower geodetic rate estimates to be unlikely, and we do not include them in our range of possible slip rates. We use $36^{\dagger}$ $\pm8^{\dagger}$ mm/yr to describe the San Andreas slip rate, in accordance with *Weldon et al.* [1993]. Orientation of the San Andreas fault is well constrained in this region at N64°W† $\pm2°^{\dagger}$.

Rotation of the San Gabriel block. Although the strike of the San Andreas fault is well defined at any point in the vicinity of our path crossing, the fault is rather curved through the Transverse Ranges. As noted by *Weldon and Humphreys* [1986], strike-slip motion across the arcuate San Andreas fault requires a rotation of the San Gabriel block with respect to the Mojave. We use $11°^{\dagger}$ $\pm4°^{\dagger}$ to represent the vector contribution arising from San Gabriel rotation west of our crossing. This ~11° counterclockwise addition to the San Gabriel velocity (with respect to the Mojave at our crossing) represents the correction in the velocity orientation incurred by traversing from where our path crosses onto the San Gabriel block to near the western end of this block. The uncertainty includes both the possible error in estimating the curvature of the San Andreas fault (±2°), and the possibility that the San Gabriel block moves relative to the Mojave with a small component of fault-normal motion (±2°). We are aware that significant amounts of fault-normal deformation occurs near the San Andreas fault [e.g., *Weldon*, 1986; *Weldon and Springer*, 1988]. However, this deformation is attributed to local, minor undulations in the trace of the San Andreas fault in conjunction with strike-slip motion of the San Andreas fault in an orientation that is consistent with the regional, curved trace [*Saucier et al.*, 1992]. Assuming a San Andreas slip rate of 36 mm/yr, slip along this curved fault is equivalent to 4.2°/m.y. of San Gabriel block rotation. With pure strike-slip motion at our San Andreas crossing and no rotation of the San Gabriel block along the San Andreas, a 36 mm/yr slip rate would result in 7 mm/yr of convergence at the western side of the Mojave. This is considered unreasonable. Our limits allow 2 mm/yr of convergence or extension.

Rotation of the San Gabriel block has been inferred from paleomagnetic data by *Terres* [1984], *Terres and Luyendyk* [1985], and *Hornafius* [1985], who report 16° ±30° of counterclockwise rotation since 10 Ma. Greater constraint is given by *Liu* [1990], who finds 27.5 ±4.5° of counterclockwise rotation since 7 Ma. Assuming the San Andreas fault defines an arc that itself is not rotating with respect to North America (as suggested by a lack of Mojave rotation [*Weldon*, 1986; *Wells and Hillhouse*, 1989]), and that the curvature of the San Andreas fault is not changing with time, then the current San Andreas slip rate produces counterclockwise rotation at 4° ±1°/m.y. This rotation rate since 7 Ma would produce ~28° of counterclockwise rotation of the San Gabriel block, a result that is in agreement with the paleomagnetic data.

Western Transverse Ranges. West of the San Gabriel block the path crosses the western Transverse Ranges and enters the California borderland. Three major deformational components are active in the western Transverse Ranges: shortening, left-lateral faulting and clockwise rotation. While these elements probably are interrelated, we consider them separately in an attempt to establish conservative limits on deformation uncertainty.

The dominant deformation across the western Transverse Ranges is shortening oriented essentially north-south. *Yeats* [1983] proposed a rate of about 23 mm/yr, based on cross sections across the Ventura Basin region, which he believed represented most of the convergence across the region. Using similar methods, *Namson and Davis* [1988] estimate 22 ±4.5 mm/yr across this zone. *Rockwell* [1983] and *Rockwell et al.* [1984] proposed a rate of 17 ±4 mm/yr based on offset of Quaternary surfaces, and recent work on individual structures within the zone [*Yeats*, 1988; *Yeats et al.*, 1988; *Rockwell*, 1988; *Rockwell et al.*, 1988] supports similarly high rates. However, *Yeats* [1993] suggests that rates could be about half (or less) of those he proposed earlier if the reverse faults that accommodate shortening do not flatten into a midcrustal detachment surface, as assumed in earlier work [*Yeats*, 1981], and a critical age estimate is corrected to be consistent with recent evidence [*Ponti et al.*, 1993]. Rates of shortening estimated with geodetic data yield a rate of 11 ±3 across the western Transverse Ranges near the Ventura Basin [*Feigl et al.*, 1993; *Donnellan et al.*, 1993], consistent with the revised geologic estimate. We use as our best estimate 11† mm/yr, a rate consistent with the various rate data. To include the great range of possible rate, we assign uncertainty limits of +10-3† mm/yr. We chose N10°E† as the direction of shortening because it is roughly perpendicular to the trends of the major folds and faults [*Yeats et al.*, 1988] and because it is similar to the orientation of N17°E estimated by *Jackson and Molnar* [1990]. We are not aware of any piercing lines across the zone to confirm the actual direction of shortening. For this reason we assign large errors of ±20°† to the deformation vector. This allows either true shortening between N10°W and N30°E, or, for shortening directed N10°E, up to 7 mm/yr of associated strike-slip shear.

Faults near the northern edge of the western Transverse Ranges, including the Santa Ynez and Big Pine faults, accommodate left-lateral slip [*Dibblee*, 1982; *Jennings*, 1974; *Luyendyk et al.*, 1980; *Hornafius*, 1985; *Clark et al.*, 1984]. Additional unrecognized left-lateral shear may occur across the western Transverse Ranges, particularly in areas undergoing strong shortening. We are not aware of good slip rate estimates for these faults, so we arbitrarily assign a cumulative rate of 2† ±2† mm/yr to reflect the consensus that they may accommodate a few millimeters per year of slip. We include the possibility of no left-lateral slip because recent work suggests that the Santa Ynez fault, a member of this group, is currently not slipping in a strike-slip manner [*Namson and Davis*, 1988; R. S. Yeats, personal communication, 1989]. The average orientation of these faults is N85°E†, with a range of +10°-20°†. Including this 2 mm/yr of left-lateral deformation is similar to rotating the direction of convergence ~12° clockwise from the N10°E direction assumed above (for our estimated convergence rate of 11 mm/yr).

The final component of deformation in the western Transverse Ranges results from clockwise rotation, which we infer is ongoing. *Luyendyk et al.* [1980, 1985] and *Hornafius* [1985] document an average rotation rate for the western Transverse Ranges and the Channel Islands of ~4°/m.y. since 15 Ma, and apparently lower rates since ~5 Ma. They account for this with a model in which the Transverse Ranges/Channel Islands blocks rotate counterclockwise within a zone of NW trending, elongated blocks accommodating regional right-lateral shear. In this model the western Transverse Ranges/Channel Islands blocks are separated from the NW trending blocks by left-lateral faults. *Jackson and Molnar* [1990] estimate a rotation rate of 6 ±3°/m.y. using a similar block model and VLBI data, suggesting that rotation is ongoing. However, as discussed in the "kinematics of Pacific-North America interaction" section, we believe that the VLBI stations they use (VAND and JPL, Figure 12) are in regions not representative of the kinematics of the Ventura Basin region. Furthermore, while this kinematic description may have been valid when right-lateral shear was concentrated in the outer continental borderland, the low rates of current activity across left-lateral faults within the western Transverse Ranges and the paleomagnetic data for recently decreasing rotation rates argue against high rates of ongoing rotation at the longitude of the Ventura Basin. We choose a rotation rate of 2 ±2°/m.y. to describe western Transverse Ranges rotation. This allows the possibility of no rotation, and the average paleomagnetic rate since 15 Ma. This rotation rate is associated with a velocity vector of 2† ±2† mm/yr directed N95°W† ±30°† for a pole near the latitude of the Transverse Ranges. The net relative velocity vector for the western Transverse Ranges path is 13 +5-3 mm/yr N10°E ±25° (at 90% confidence).

The end-of-path relative velocity vector calculated for the Transverse Ranges path is 46 ±5 mm/yr oriented N50°W ±7°. The uncertainty bounds are given at the 90% confidence level.

Peninsular Ranges Path

Rio Grande. Like the Transverse Ranges path, the first significant deformation encountered along this path is associated with the Rio Grande Rift. Published slip rate estimates exist only for the central portion of the rift, east of the Colorado Plateau, and have been discussed above with respect to the Transverse Ranges path. The long-term average extension rate there is ~0.2 mm/yr, and the late Quaternary rate is inferred to be ~0.14 mm/yr [*Golombek*, 1981; *Golombek et al.*, 1983].

The Peninsular Ranges path crosses the rift south of the central rift, in a region where the rift and the major faults within it trend north. Therefore we assume that extension occurs N90°W†, perpendicular to this trend. As discussed under the Transverse Ranges path discussion above, we assign an uncertainty in orientation of ±30°†. Given the southward increasing net extension and the estimated Quaternary extension rate for the central rift, a simple extrapolation of rate to where the Peninsular Ranges path crosses the rift yields 0.25† mm/yr, which we use for our best estimate. As bounds to the extension rate we use the lowest central rift estimate (0.1† mm/yr) and the maximum central rift estimate with a linear extrapolation in rate to the south (0.5† mm/yr).

Southern Basin and Range. The southern path crosses approximately 750 km of Basin and Range between the Rio Grande Rift and the San Andreas fault. The large number of poorly studied structures there makes estimating deformation rate difficult. There have been 6–7 scarp-producing earthquakes in southeastern Arizona during the past 15,000–20,000 years [*Menges and Pearthree*, 1983; *Pearthree et al.*, 1983; *Pearthree*, 1986], suggesting a rate of a few tenths of a millimeter per year across that zone. While there are a few late Quaternary scarps and scattered seismicity along the southern path in south central and southwest Arizona, it is unlikely that those areas add significantly to the total deformation [*Pearthree*, 1986].

Considering the region as a whole, most workers agree that the southern Basin and Range is currently 1–2 orders of magnitude less active than the northern Basin and Range [e.g., *Stewart*, 1978; *Greensfelder et al.*, 1980; *Zoback, et al.*, 1981; *Pearthree*, 1986]. As discussed with respect to the Sierra Nevada path, the northern Basin and Range is extending at 5–15 mm/yr, which suggests a southern Basin and Range rate of between 0.05 (zero for our purposes) and 1.5 mm/yr. A similar estimate could be inferred from the consensus that current southern Basin and Range extension occurs at a rate that is 1–2 orders of magnitude less than the 13 Ma average. Assuming 15% of net extension across the 750 km of southern Basin and Range since 13 Ma yields an average rate of ~7 mm/yr. One to 10% of this rate is ~0–1 mm/yr.

Choosing a rate that is intermediate within this range of estimates, we use 0.5† mm/yr as our best estimate for the net extension rate along the southern path between the Rio Grande Rift and California, with a range from 0.25† to 1.0† mm/yr. The most active faults in the southern Basin and Range are normal faults that trend north to NNW [*Menges and Pearthree*, 1983]. Other faults that may contribute a small amount of deformation trend NW to NNW. We take N100°W† as our preferred direction and assign an error of ±30°† to accommodate the range of fault trends and the possible occurrence of oblique extension.

California east of the San Andreas fault. We include southern Basin and Range faulting near the California border with the deformation estimate for extension across the southern Arizona Basin and Range. Deformation there since ~5 Ma is minor [*Buising*, 1992; *Richard et al.*, 1992] and is not likely to influence our path-integrated velocity estimate by a significant amount. The region east of the San Andreas fault is an area broken by east trending left-lateral faults and north to NW trending normal faults. It has been suggested [*Richard and Dokka*, 1992] that this region is part of the eastern California shear zone recognized farther north [*Dokka and Travis*, 1990]. Little evidence exists for the occurrence of deformation in this region at rates similar to those found farther north, and we think that the eastern California shear zone is more closely associated with the San Andreas fault in the vicinity of the eastern Transverse Ranges (although earlier it may have been concentrated farther east). This idea is supported by geodetic observations across the southern Mojave that indicate much greater strain rates in the western Mojave than in the eastern Mojave [*Savage et al.*, 1990]. However, earthquake activity east of the San Andreas fault suggests some right-lateral activity on the NW trending faults and some left-lateral activity on the east trending faults. The east trending faults appear to be more important, and these have been used to describe a regional deformation where the blocks they bound rotate clockwise, producing ~40° of paleomagnetically inferred rotation since ~12 Ma [*Carter et al.*, 1987]. An alternative model, in which left-lateral faulting between these blocks occurs as the blocks pull away from Arizona with increasing displacement to the north, seems unlikely because of the nearly undeformed ~5 Ma sediments that lie east of the east trending faults [*Buising*, 1992; *Richard et al.*, 1992]. The east trending faults have an average orientation of N100°W, and their rotation would result in a velocity at their western end oriented ~N10°W (with respect to their eastern end). Any right-lateral activity on the NW trending faults would result in a more westerly orientation for the velocity just east of the San Andreas fault. We choose N20°W† as our preferred orientation so as to admit some component of right-lateral deformation and so that deformation in this zone parallels the proposed eastern California shear zone in this area. To allow for a range of possible interpretations for the deformation in this region, we assign a wide uncertainty of +30°-20°†.

The length of the east trending faults (and the blocks they bound) decrease to the south; at the latitude of our path they are ~70 km long. If these blocks have been rotating at a constant rate over the last 12 m.y., the velocity at the west end relative to the east end resulting in 40° of rotation is ~4 mm/yr. It seems more likely, however, that these faults are most active when they lie east of a pronounced left bend in the San Andreas fault and permit the crust there to negotiate the bend; in this case, the rate of fault activity diminishes as this crust moves south of the bend [*Powell*, 1981]. In support of this belief, deformation rates east of the northern Salton Trough appear to be greatest within 10 km of the San Andreas fault across a zone of north to NW trending normal faults that displace by only a few meters the same late Quaternary surfaces offset hundreds of meters by the San Andreas fault [*Clark et al.*, 1984]. This observation implies that these faults contribute less than a few tenths of a millimeter per year. By considering the set of data for deformation in California east of the San Andreas fault, a net velocity of 2–3 mm/yr would be a conservative maximal estimate for deformation over this broader region. For the velocity incurred by crossing eastern California in the vicinity of our path, we assign a best estimate of 1† mm/yr, and limits that include no† motion and 3† mm/yr.

Each of the three deformation regions encountered east of the San Andreas fault (the Rio Grande Rift, the southern Basin and Range, and eastern California) is probably deforming at less than 1 mm/yr. For the combined region, we calculate that between 0.3 and 2.0 mm/yr of net velocity is accumulated oriented N44°W ±45°, with a best estimate of slightly over 1 mm/yr. While it is difficult to quantify this small amount of deformation, it should be clear that the overall style is extension in the direction of our path at rates very low compared to the other rates encountered along the path farther west.

San Andreas fault. The Peninsular Ranges path crosses the San Andreas at a place where the fault zone is fairly simple, where the best slip rate data exist and the fault trend is well constrained. *Sieh* [1986; also personal communication, 1988] has inferred a slip rate of ≥ 30 mm/yr based on 21 m of offset caused by at least four earthquakes between 1000 and 1700 A.D. The actual average slip rate may be greater than 30 mm/yr because displacement across at least one strand of the fault is not included in this estimate [*Sieh*, 1986]. However, because *Sieh* [1986] infers that an earthquake occurred at both the beginning and end of the measured interval, it is also possible that the average rate is overestimated by an amount associated with the displacement of one earthquake. We use Sieh's estimate of 30† mm/yr as the best estimate and include an error of ±7† mm/yr to accommodate these counterbalancing possibilities. This rate estimate is supported by the work of *Keller et al.* [1982], who, on the basis of an offset fan crossing the fault just north of where our path crosses the San Andreas fault, determine a rate of 10–35 mm/yr, with 23–35 considered "most likely." Geodetic measurements of the slip rate fall in this range as well [e.g., *Savage*, 1983]; however, the short time interval represented by these measurements and the difficulty of separating the strain associated with the San Jacinto fault makes it difficult to use the geodetic data to constrain the San Andreas fault strain-rate estimate.

We use N48°W† with uncertainties of +7°-3°† for the vector representing San Andreas slip orientation. This assumes pure right-lateral slip across the average trend of the zone, with uncertainties representing the range of trends found for the fault nearby. North and south of our crossing point there are recently uplifted hills that have been interpreted as indicating transpressive motion across the San Andreas fault [e.g., *Sylvester and Smith*, 1976]. We infer that these structures result from geometric complexities in the local fault zone structure rather from regional transpression. A potentially more serious problem may be the occurrence of extension across the Salton Trough as a whole. Our best slip vector is based on the assumption that the depression is due entirely to a pull-apart mechanism, as is widely believed [e.g., *Elders et al.*, 1972; *Crowell and Sylvester*, 1979], but if a component of extension perpendicular to the trend of the San Andreas fault occurs, our vector should trend more westerly. The range of trends allowed by our assigned uncertainty for the San Andreas slip vector allows nearly 2 mm/yr of fault-normal contraction and 4 mm/yr of extension.

San Jacinto fault. The next fault encountered along our path is the San Jacinto, which is crossed at a location where the fault zone is relatively simple (consisting essentially of one branch), and there are a number of relatively consistent slip-rate estimates. *Sharp* [1981] proposed a minimum rate of 8–12 mm/yr based on the offset of gravels containing the 0.7 Ma Bishop ash. We infer from his discussion of the relationships that the actual slip rate value is likely to be close to this range. More recent work in the area [*Rockwell et al.*, 1986b; *Merifield et al.*, 1987] suggests an offset rate of 12–14 mm/yr for many latest Pleistocene and Holocene deposits and surfaces. Because of the consistency among these rates and our interpretation of Sharp's long-term rate, we use 12† mm/yr as our best rate estimate. *Sharp* [1981] argues that the short-term slip rate varies, and he estimates rates as low as several millimeters per year for the past several thousand years. We do not include these low numbers in our estimate because they were derived from other portions of the fault, where the fault zone is more complex and where we believe additional distributed deformation is occurring. (That is, we infer that rate variability across San Jacinto fault zone is spatial rather than temporal, and probably represents varying fractions of the total deformation accommodated off the main trace.) In either case, we follow our overall philosophy of using the longer-term rate at the simplest site. We assign a rate uncertainty of ±4† mm/yr to our rate estimate of 12 mm/yr.

The San Jacinto fault strikes N53°W† where crossed by our path. Offset features nearby are consistent with pure strike-slip there [*Sharp*, 1981; *Rockwell et al.*, 1986b; *Merifield et al.*, 1987]. The San Jacinto fault zone consists of a series of what appear to be pull-apart valleys between overlapping right-stepping fault segments that trend from about N43°W to N58°W. This range yields limits on our preferred trend of +5°-10°†. The trend at at our crossing is 5° more westerly than the trend of the zone as a whole [N48°W, *Sharp*, 1967], which is consistent with the observed slightly transtensional nature of the fault zone as a whole.

Elsinore fault and nearby faults to the east. Between the San Jacinto and Elsinore fault zones lie a number of poorly characterized NW trending fault zones (not shown on our figures), including the Hot Springs, Agua Caliente, San Felipe, and Earthquake Valley fault zones. Although we know of no published slip rate estimates for these zones, portions are considered active [*Jennings*, 1974; *Rockwell et al.*, 1989]. As a set these faults form a broad zone trending N58°W ±20° connecting the southern San Jacinto with the northern Elsinore fault zones and perhaps transferring slip from the Salton Trough to the northern Elsinore fault zone. Given the similar trend of these faults with known right-lateral faults in the area, we expect that these faults are predominantly right-lateral. *Rockwell et al.* [1989], however, discuss left-lateral slip on at least one strand of this fault zone. By comparison with the morphology of the Elsinore and San Jacinto faults we infer that this zone contributes less than 1 mm/yr of slip. To include the possibility of either left- or right-lateral slip, we assign a slip rate of 0 ±1 mm/yr. For presentation purposes, we include this slip with the Elsinore fault.

Our path crosses the Elsinore fault near where *Vaughan and Rockwell* [1986] have proposed a slip rate of 5 mm/yr with uncertainties of +1 -2 mm/yr. This rate is comparable with other slip rate estimates along the fault produced by this group [e.g., *Pinault and Rockwell*, 1984; *Rockwell et al.*, 1986a]. These estimates are on the high end of the range of earlier published estimates, which range from 1 mm/yr [*Ziony and Yerkes*, 1984] to 7 mm/yr [*Kennedy*, 1977]. In every study, however, the fault zone was found to be complex, and few absolute dates have been reported. We use the best estimate of *Vaughan and Rockwell* [1986] from their site near our path (i.e., $5^{\dagger}$ mm/yr), but extend the uncertainty to +2-4 mm/yr to accommodate the range in published rates. Where the southern path crosses the Elsinore, the fault undergoes several changes in trend. The average trend there is about N49°W†, which is comparable to the average trend of the zone as a whole. Individual faults deviate +18° -10° from this orientation. Convolving the Elsinore velocity probability field with that of the NW trending faults between the San Jacinto and Elsinore faults mentioned above results in slightly greater uncertainty: rate uncertainty limits of +3-5† mm/yr and orientation uncertainty limits of +20°-12°†.

Rotation of southern California blocks. The trace of the San Andreas fault zone is distinctly curved south of and through the Transverse Ranges. Discounting stepovers and other local geometric complexities, the curvature is remarkably constant from the western termination of the Garlock fault to the Mexican border, including the Imperial fault (Figure 1b). As pointed out by *Weldon and Humphreys* [1986], pure strike-slip motion along this curved trace produces a counterclockwise rotation of the crust SW of the fault, and motions associated with this rotation should be estimated and included in our path integration. Taking the San Andreas fault as the northern boundary of the rotating region, once the integration path crosses the San Andreas fault the San Andreas-related velocity will decrease as the Euler pole is approached, and where the path has a component that is parallel to curved San Andreas fault, this vector will rotate as the path is traversed.

As discussed under the Transverse Range path, the San Gabriel block probably rotates at a rate implied by slip along the curved San Andreas fault. If the blocks south of the San Gabriel block were not rotating with the San Gabriel block, a "jaw-like" effect would occur, whereby north directed shortening would occur with an increasing rate toward the west. This results in a greater convergence rate north of the Los Angeles Basin and across at least the eastern portion of the western Transverse Ranges, relative to the central Transverse Ranges, as is observed. Complicating the situation, however, is the similar effect produced by right-lateral slip on the San Jacinto, Elsinore, and Newport-Inglewood faults, which also causes increasing rates of thrusting to occur toward the west. In lieu of a thorough analysis of the combination of effects, we simply assume that rotation of the entire region north of the San Miguel and Rose Canyon fault systems is occurring at half the rate implied by the curvature and rate of slip on the San Andreas fault, whereas the San Gabriel block rotates at the full rate implied by the San Andreas kinematics. As limits we choose a possible range of rotation that includes both no rotation and full rotation of this region.

To complete the path west of the Elsinore fault, we estimate the velocity resulting from two independent paths (Figures 2 and 4) that end in the southern California borderland. One path heads south into northern Baja before heading offshore and back to the southern California borderland, and the other path heads directly toward the assumed southern California pole of rotation and into the borderland (see Figure 2). The first path uses the rate information determined for the northern Baja faults but has poor orientation constraint owing to uncertainties in the rotation rate of these blocks. The second path has better orientation control because it trends toward the pole, so block rotation does not affect the orientation. However, rate information is poor along this path. When convolved together, these two paths result in a well constrained estimate.

The velocity contributed to a path integral by crossing a region experiencing rotation depends on the locations where the path enters and leaves the rotating block. The vector associated with the block rotation for the southern California option, including contributions for radial and tangential path segments, is $3.5^{\dagger}$ $\pm 3.5^{\dagger}$ mm/yr oriented N132°E† ±10°†. This orientation is very near to that of the southern California faults and hence does not degrade seriously the uncertainty in orientation. The correction vector for the northern Baja option is $4^{\dagger}$ $\pm 4^{\dagger}$ mm/yr oriented N83°E† ±20°†.

Northern Baja faults. The San Miguel-Vallicitos and Agua Blanca fault zones (Figure 1b) are the two main onshore zones crossed by the southern path in Mexico. The San Miguel-Vallicitos is a zone of seismic activity that has received very little field work. On the basis of its morphology and trend, which is parallel to the Agua Blanca fault, it is likely to be a slightly active right-lateral fault. Because little is known about this fault, we arbitrarily assign a rate of $1^{\dagger}$ $\pm 1^{\dagger}$ mm/yr, based solely on its seismicity and morphology. It trends N55°W† ±8°†. The Agua Blanca fault is a major right-lateral fault [*Allen et al.*, 1960], connecting the California borderland to the Gulf of California. Preliminary work on the late Quaternary slip rate of the main trace suggests a rate of about 4 mm/yr [*Schug et al.*, 1987; *Hatch and Rockwell*, 1986], with the possibility of 1-2 mm/yr on the other strands thought to be important (T. K. Rockwell, personal communication, 1987). On the basis of their work we assign a rate of 5† ±2† mm/yr to the northern and main strand, and include 1† mm/yr to the upper uncertainty estimate to account for possible deformation beyond that measured on these traces. In the region where the fault is a simple zone the average trend is N67°W†, though individual segments trend +10°-5°† from this.

Our path continues west across the continental borderland just south of the Mexican border. Once offshore there is little information other than the seismicity and morphology of the faults with which to estimate styles and rates of activity. Using detailed topography determined from Seabeam surveys, *Legg* [1991] and *Legg et al.* [1989] have documented on offshore faults many of the classic morphologic features associated with active strike-slip faulting, including pull-aparts, rift valleys, scarps, and shutter ridges. *Legg et al.* [1991] note that the Agua Blanca fault zone joins the offshore inner borderland faults near the coast and that there is another independent system of active faults, associated with the San Isidro fault, connecting California borderland faults farther to the west with faults along the Pacific margin of Baja. Seismicity and documented faulted offsets of late Quaternary deposits along the Baja coast [*Yeats and Haq*, 1981] provide additional evidence for the occurrence of deformation west of Baja. From Legg's work we infer that this outer system is active in a right-lateral sense, and on the basis of its modest seismicity we assign 2† mm/yr of slip. Because this is little more than a guess, we assign a large uncertainty of ±2† mm/yr, which includes, as a limit, no motion. The trend of the faults west of the Agua Blanca is N32°W† ±8°. If these are pure right-lateral strike-slip faults, this is the trend of the velocity vector representing their deformation. From Legg's work we infer that motion on these faults is nearly pure strike-slip. However, to include the possibility of a normal component of slip to produce the distinctive extensional morphology of the borderland, we add an additional 7° to the western limit of the direction of motion (for a total of 15°†), and to include the possibility of a thrust component, as suggested by thrust mechanisms found in the borderland farther north [e.g., *Pacheco and Nabelek*, 1988], we include an additional 7° to the northern limit (for a total of 15°†). Effectively, our best vector for motion on this fault system allows pure right-lateral strike-slip motion across the average trend of the faults, and the range of uncertainty allows up to 25% convergence and extension.

The velocity estimate for faults west of the Elsinore provided by this path is 5.5 ±1.9 mm/yr oriented N32°W +20°-30°. The uncertainty bounds are given at the 90% confidence level.

California faulting west of the Elsinore fault. We also determine a velocity estimate for a path option that heads SW from the point of Elsinore fault crossing, accumulating deformation on the faults thought to be kinematic continuations of the northern Baja faults [*Legg et al.*, 1991]. Good orientation information exists for these faults [*Legg*, 1991; *Legg et al.*, 1989, 1991], but no reliable estimates exist for the slip rates of these faults. We include velocity information for the Rose Canyon, Coronado Bank, and San Diego Trough fault systems, which Legg describes as kinematic continuations of the northern Baja faults. Because there is very little rate control, we allow a wide range of possible rate: a preferred rate of 1† mm/yr on each fault system, a minimum rate of 0.5† mm/yr, and a maximum rate of 3† mm/yr on the Rose Canyon and Coronado Bank systems and 4† mm/yr on the San Diego Trough (a higher rate because of the relatively pronounced physiography associated with this fault). Orientations are: N37°W† ±7°† for the Rose Canyon fault zone, N33°W† ±7°† for the Coronado Bank fault zone, and N32°W† ±6°† for the San Diego Trough fault zone. We also include a velocity vector for the San Clemente fault, which is known to be seismically active, but which is inferred to be kinematically independent of the northern Baja and inner borderland faults. As with the other borderland faults, its orientation is well constrained, N46°W† ±5°†, and its rate is poorly constrained. The rate of seismicity of the San Clemente fault appears to be greater than any of the inner borderland faults but significantly less than the seismicity of the combined set of inner borderland faults. To admit this wide range, we represent San Clemente activity with 2† mm/yr +5-1.5† mm/yr. This allows a range of slip from 0.5 mm/yr to 7 mm/yr.

The velocity estimate for faults west of the Elsinore provided by this path is 4.4 ±3.0 mm/yr oriented N32°W +9°-18° (at 90% confidence).

By determining each Peninsular Range-to-borderland subroute independently and taking the product of their uncertainty distributions (Figure 4) we have an estimate for the rate of deformation over this portion of the plate boundary of 5.3 ±1.7 mm/yr at N29°W +7°-9° (at 90% confidence), where a minor 1.4° clockwise rotation of the northern Baja vector has been made. This is the correction needed to bring the end of the Baja path option to the southern California borderland along a NUVEL-1 or RM2 Pacific-North America small circle. Our estimate is comparable with both our borderland and northern Baja faults slip rate estimates. *Anderson* [1979] infers a combined rate of ≤10 mm/yr for the same region, based on seismicity.

By convolving the estimate for motion west of the Elsinore fault with the estimate for motion across and east of the Elsinore fault we arrive at a net end-of-path estimate for the southern path of 52 ±6 mm/yr oriented N48°W ±2° (uncertainties given at the 90% confidence level). This result is represented graphically in Figure 3.

Sierra Nevada Path

In this section, Pacific-North America relative plate motion is estimated by considering deformation along a path that crosses the active southern Great Basin, the San Andreas fault where its behavior is relatively simple, and a complex zone of shortening and lateral shear east and west of the San Andreas fault (Figure 2). This is kinematically equivalent to the route considered by

Minster and Jordan [1984]. To help assess the error associated with this path where it crosses the SW Great Basin, we also consider a path that leads south out of southern Nevada and into the Mojave and then crosses the western Garlock fault, joining the main path in the Sierra Nevada.

East of California. At the northerly latitude of this path, Rio Grande Rift extension is nearly absent. By extrapolating the rates discussed in the previous paths to the location in south central Colorado where this path crosses the rift, we infer a rate of 0.05 † ±0.05 † mm/yr oriented to the west † ±30° †. The velocity contribution provided by Colorado Plateau rotation is the same as that discussed under the Transverse Ranges path: 0.1 † ±0.1 † mm/yr directed to the north † ±30° †. The net velocity resulting from Rio Grande rifting and Colorado Plateau rotation is 0.11 ±0.10 mm/yr oriented N30°W ±30°.

Deformation within the Great Basin is heterogeneously distributed. Northern Great Basin extension is currently concentrated in three zones: the Wasatch and Sierra Nevada fronts and the central Nevada seismic zone [*Wallace*, 1984; *Eaton et al.*, 1978]. Seismicity occurring near the Wasatch Front is part of a seismically active belt that coincides with the Great Basin margins to the east (the southern intermountain seismic belt [*Smith and Sbar*, 1974]) and south [*Smith*, 1978]. *Schwartz and Coppersmith* [1984] estimate an extension rate of ~1 mm/yr on the Wasatch Front. However, the VLBI station ELY in NE Nevada appears to be moving N98°W at 4.9 ±1.3 mm/yr Dixon et al. (submitted manuscript, 1994), and the Wasatch Front represents the only kinematically important feature known between stable North America and ELY. Hence additional deformation may be occurring near the Wasatch Front or in the eastern Great Basin. Our path crosses the eastern margin of the Great Basin in SW Utah. Deformation there occurs on a family of predominantly normal faults near the western margin of the Colorado Plateau, and the most active of these faults is the Hurricane [*Hamblin et al.*, 1981; *Mayer*, 1986]. From this work we infer a rate of about 1.0 ±0.5 mm/yr for the entire zone bounding the western Colorado Plateau. Motivated by the geodetically inferred motion of ELY and its apparent contradiction with the geologic data, we include the possibility of additional deformation near this frontal system of faults or in the southern Great Basin by choosing a rate of 2.0 † +3.0-1.5 † mm/yr. This allows rates as great as the inferred motion of ELY and as low as 0.5 mm/yr. Faults trend essentially to the north where our path crosses this fault zone, suggesting a westward † extension direction. As we have done above in characterizing extensional zones, we assign ±30° † from this direction to permit for oblique extension. Net deformation to this point in southern Nevada is 2.1 +2.1-1.1 mm/yr directed N86°W ±22° (at 90% confidence).

Great Basin option. The western portion of the Great Basin, where crossed by our path, consists of an actively deforming, triangular-shaped region (Figure 1b) delineated by the Sierra Nevada on the west side and the Death Valley fault system on the east side. The Garlock fault commonly is believed to define the southern limit of this active extensional domain [*Davis and Burchfiel*, 1973]. This region is characterized by relatively high rates of extension (compared to the Great Basin as a whole), the presence of NNW to NW trending faults which accommodate relatively high rates of right-lateral shear [*Stewart*, 1988; *Burchfiel et al.*, 1987; *Lubetkin and Clark*, 1988], and a kinematic relationship to the Garlock fault and deformation occurring in the Mojave Desert [*Sauber*, 1989; *Dokka and Travis*, 1990].

The Death Valley region is the first zone of ongoing deformation encountered along our path within California. Death Valley graben formation has been attributed to extension across a right step between the right-lateral Furnace Creek and Death Valley fault zones [*Burchfiel and Stewart*, 1966; *Wright et al.*, 1974; *Troxel and Wright*, 1987], though the southern Death Valley fault zone may accommodate only a fraction of the slip experienced by the northern Death Valley/Furnace Creek fault system [*Stewart*, 1988]. Unfortunately, the best rate estimate is associated with the southern Death Valley fault system. *Butler et al.* [1988] estimate ≥ 3.5 mm/yr across this zone for the duration ~11–1 Ma, consistent in rate with the ~80 km of late Cenozoic displacement inferred for the Panamint Mountains block on the Furnace Creek fault zone [*Stewart*, 1988]. However, *Butler et al.* [1988] find the southern Death Valley fault zone to be nearly inactive since ~1 Ma. Across the northern Death Valley and Furnace Creek fault zones, *Clark et al.* [1984] estimate a Quaternary slip rate of ~1 mm/yr, which is consistent with the geomorphology there.

We use the 1 † mm/yr slip rate estimate of *Clark et al.* [1984] to characterize the current slip rate of the Furnace Creek-Death Valley fault system. This rate is intermediate to the range of possible values and is suggested by the Quaternary estimate. To represent the wide range of uncertainty in the slip rate estimate, we use values that include both no † slip and slip at 4 † mm/yr (to admit Butler's ~10 m.y. average, where we must assume that since 1 Ma, nearby features presently accommodate the deformation). Orientation of the major strike-slip elements comprising the Death Valley-Furnace Creek system is N47°W † ±8° †.

The next active documented zone encountered along our path is the Hunter Mountain fault system. This system is associated with Saline and Panamint Valleys, both of which are considered by *Burchfiel et al.* [1987] to be pull-apart basins similar in kinematic origin to Death Valley. These researchers estimate a displacement of 8-10 km since ~3 Ma, yielding an average rate of 3 † ±1 † mm/yr. Where the system is strike-slip in nature it trends N57°W † ±6° †. This rate is similar to the Holocene slip rate of 2.4 (uncertainty of ±0.8 mm/yr) found by *Zhang et al.* [1990] for the southern Panamint Valley fault zone, which is the southern continuation of the Hunter Mountain fault zone. The trend of the Panamint Valley fault zone is nearly to the north, though local topography suggests that nearby normal faults are active (as is required by the pull-apart model for the origin of the valley).

Lubetkin and Clark [1988] have documented a Holocene right-lateral slip rate of 1-2 mm/yr across the Owens Valley fault zone, and they suggest that this zone is the most active of the strike-slip Owens Valley faults. This value is less than the 3 to 7 mm/yr rate inferred from geodetic studies [*Savage et al.*, 1975; *Savage and

Lisowski, 1980]. We use the Holocene slip rate estimate, consistent with our convention of choosing such data when they are available. The orientation of this fault zone is N12°W ±8°. While the Owens Valley earthquake of 1872 created significant vertical relief [*Lubetkin and Clark*, 1988], this fault is essentially strike-slip in nature [*Beanland and Clark*, 1987]. The southern Sierra Nevada frontal system is dominated by normal slip [*Gillespie*, 1982]. However, this deformation is documented to be less active than the Owens Valley strike-slip activity by at least an order of magnitude [*Clark et al.*, 1984; *Zoback*, 1989]. Thus deformation in the Owens Valley region is dominated by the Owens Valley fault, and, accordingly, we assign a velocity to the deformation across this region of 1.5† mm/yr +1.0-0.5† mm/yr, N17°W† +20°-13°†. The five additional westerly degrees accommodate possible normal extension at a rate ~10% that of the Owens Valley fault strike-slip rate, and orientation limits have been widened to allow a range in frontal fault extension rate from zero to 0.5 mm/yr. The resultant estimated motion of the southern Sierra Nevada with respect to the point where this path crosses the California-Nevada border (i.e., the Great Basin option, Figure 7b) is 8.2 ±1.8 mm/yr N57°W ±7° (at 90% confidence). Including the deformation to the east yields an estimated velocity for the Sierra Nevada with respect to North America of ~10 mm/yr N60°W.

An estimate of Sierra Nevada motion averaged over 15 m.y. is available by reconstructing late Cenozoic offsets in the region between the southern Sierra Nevada and the Colorado Plateau [*Wernicke et al.*, 1989]. This calculation yields an average extension rate of 16.7 ±4.5 mm/yr N73°W ±12°, which Wernicke et al. use to argue that the extension rate has slowed and reoriented, with extension in the last ~4 m.y. concentrated in the region west of the California-Nevada border and in a more northerly direction.

Mojave/Garlock option. An alternative Sierra Nevada block velocity estimate is obtained by leaving the original Sierra Nevada path in southern Nevada, crossing the southern Nevada portion of the intermontain seismic belt and the NE trending, left-lateral Lake Mead fault system, following the Colorado River to California, heading west across the Mojave, and finally heading north across the Garlock fault to the Sierra Nevada. The active fault systems in southern Nevada are complex, expressing normal, strike-slip and thrust styles of deformation [*Anderson and Barnhard*, 1993]. This region is one of transition between the active Great Basin and the nearly inactive southern Basin and Range, and these faults probably help accommodate this difference. *Anderson and Barnhard* [1993] find a N105°W direction of extension in the Mormon Mountains portion of the intermountain seismic belt (in eastern Nevada, west of the Utah-Arizona border), which is similar to the overall trend in seismicity that defines this belt [*Smith*, 1978]. The Lake Mead fault system has been active in the last 5 m.y., offsetting the now inactive Las Vegas shear zone [*Anderson et al.*, 1972; *Bohannon*, 1984] and producing scarps in Pleistocene alluvium. Its trend is approximately N130°W. To allow for the possibility of significant activity on these zones, we assign a velocity of 1† ±1† mm/yr N65°E† ±25°†. This orientation is intermediate to the two active zones, giving slight preference to the intermountain belt because of its greater seismicity. In the maximum limit, this rate is as great as our best estimate for extension in the vicinity of the Hurricane and fault system (discussed above in this section). This uncertainty range also allows the possibility of no activity. The next significant activity encountered is that in the eastern Mojave, which is discussed in the section above that discusses the Transverse Ranges path (8.0† +3-4† mm/yr N15°W† ±25°†).

The Garlock fault slip rate near the SW corner of the Great Basin is estimated at ~7 mm/yr [*Clark and Lajoie*, 1974; *Astiz and Allen*, 1983; *Pampeyan et al.*, 1988]. We [*Weldon and Humphreys*, 1986] had inferred from the work of *Carter* [1980; 1982] that the rate was about 11 mm/yr. However, more recent work has led B. A. Carter (personal communication, 1988) to conclude that the offset units upon which his estimate is based are older than he had thought earlier, requiring a lower slip rate consistent with other estimates. We use 7 mm/yr as our best estimate of Garlock slip rate, which is used to describe the relative motion between the southern Sierra Nevada and the Mojave block. However, this velocity is derived from the location where slip rate estimates are available, and slip there depends upon the local kinematic role played by the Garlock fault. Two important kinematic processes may contribute to this velocity: (1) The Garlock fault may accommodate extension in the Great Basin, allowing the Sierra Nevada to move relative to the Mojave in a direction that is parallel to the trend of the Garlock fault [*Davis and Burchfiel*, 1973]. Because neither the rotation of the Mojave [*Wells and Hillhouse*, 1989] nor the Sierra Nevada [*Argus and Gordon*, 1990, 1991] is thought to occur at rates great enough to contribute significantly to Garlock fault slip, the slip rate of the Garlock fault where it separates the Sierra Nevada from the Mojave is thought to represent this role. Figure 13 shows this in a North America frame of reference: the displacement across the eastern California shear zone causes the western Mojave to move approximately to the north, while the addition of Great Basin extension north of the Garlock fault produces a northwest direction of motion of the Sierra Nevada (Figure 13). (2) Garlock fault activity may be involved with deformation occurring across the eastern California shear zone, which trends through the region of the eastern Garlock fault [*Dokka and Travis*, 1990]. In this role, the Garlock fault would be one of several left-lateral west trending faults in the NW Mojave that accommodate clockwise rotation of blocks they bound. Hence this component of Garlock slip would be confined to the region where important block rotation is occurring, which presumably is defined by the longitudinal range of the west trending faults in the NW Mojave that lie south of the SW Great Basin.

The Garlock fault slip rate estimate that we use (i.e., the values of ~7 mm/yr) comes from an area that lies west of the mapped west trending faults in the NW Mojave that is near the section of fault that bounds the southern Sierra Nevada. We therefore think that this slip rate estimated for the Garlock fault receives relatively little contribution from deformation occurring across the eastern California shear zone and probably represents

Sierra Nevada-Mojave relative motion well. We use the trend of the Garlock south of the southern Sierra Nevada (N125°W) to give the orientation of the relative motion vector. However, because the location from which this estimate is derived lies east of the Sierra Nevada and because the fault trend there is more west trending than it is in the region where the Garlock fault more clearly represents Sierra Nevada-Mojave relative motion, we are not certain that some of the estimated slip is not related to activity associated with the eastern California shear zone.

To handle this problem, we first assume that our velocity estimate of 7 mm/yr N125°W describes southern Sierra Nevada-Mojave relative motion, and we assign uncertainty limits under this assumption. We then consider that some component of Garlock slip at the location of the rate estimate is due to eastern California shear zone activity, and because this correction is small, we simply modify our previous estimate to accommodate this. Uncertainty limits on the rate are made wide enough to include a minimum rate of 3 mm/yr (given by the minimum creep rate estimate for the western Garlock fault [*Louie et al.*, 1985]) and a maximum of 11 mm/yr (inferred from the initial work of *Carter* [1980, 1982]). The observed trend of the Garlock fault where it separates the southern Sierra Nevada from the Mojave varies by +3° and -8°. This defines our uncorrected velocity estimate.

If eastern California shear zone deformation contributes to the velocity, the rate should simply be subtracted from the existing rate estimate so the deformation is not included twice (the orientation should not be affected because eastern California shear zone deformation is accommodated by faulting and rotation yielding a velocity estimated and applied above; slip on the Garlock fault is assumed here to be a part of this faulting). To include this possibility, we reduce our best rate estimate of 7 mm/yr by 2 mm/yr. There is no change in either the upper rate limit (because eastern California shear zone deformation may not contribute to slip at the site where the velocity estimate is derived) or the lower rate limit (because it represents data derived from where the Garlock bounds the southern Sierra Nevada). Diminishing the most likely rate estimate by 2 mm/yr without changing the uncertainty limits reduces the centroid of the rate probability distribution by less than 1 mm/yr. The final velocity estimate for the relative motion between the southern Sierra Nevada and the Mojave block is 5† mm/yr +6-2† mm/yr oriented N125°W† +3°-8°†.

Estimating the southern Sierra Nevada velocity (relative to point where the path crosses the California-Nevada border) by using features found along this alternate path yields a southern Sierra Nevada velocity (for the Mojave/Garlock option, Figure 7a) of 9.7 ±2.5 mm/yr N62°W ±19° (at 90% confidence). This result is about 1.7 mm/yr greater in a westerly direction than that obtained by the Great Basin option, i.e., the path that lies north of the Garlock fault yields a more westerly velocity. This difference suggests that the actual contribution to the Mojave path option by the Garlock fault may be toward the lower limit of its uncertainty distribution, which in turn suggests that most of the Garlock estimated slip rate (of 7 mm/yr) is a result of eastern California shear zone activity. Alternatively, our assumption (in the Great Basin path) that the orientation of deformation across the California Great Basin is given by what are inferred to be purely strike-slip elements may be in error. Kinematic information on the strike-slip elements is well documented, but additional, west directed extension may possibly have been neglected, thus omitting a westerly contribution to the Sierra Nevada velocity estimate. If such extension occurs, and the western Garlock fault slip rate is near the estimated rate (Table 1), then the deformation field is more similar to the "intercontinental transform" kinematics described by *Davis and Burchfiel* [1973] than the "pull-apart" kinematics presented by *Burchfiel and Stewart* [1966] and *Burchfiel et al.* [1987]. It is also possible that some of the difference between the two estimates is accommodated by complex deformation in the southern Sierra Nevada that we have not considered. If this complication is occurring, then the Great Basin estimate of Sierra Nevada motion would be more representative of Sierra Nevada/Great Valley motion as a whole because the Great Basin path enters the Sierra Nevada north of this possible zone of deformation.

We take the product of the two estimates to obtain a best velocity estimate for southern Sierra Nevada motion (relative to North America), yielding 8.6 ±2.0 mm/yr N51°W ±9° (Figure 7c). This estimate is similar to the southern Great Basin velocity estimate because the uncertainties associated with this path are smaller than those associated with the Mojave/Garlock path. The estimated Sierra Nevada velocity is inconsistent with that determined geodetically by *Argus and Gordon* [1990, 1991] (11 ±2 mm/yr oriented N28°W ±6°, with uncertainties at two standard errors), is marginally consistent with the estimates of Dixon et al. (submitted manuscript, 1994) (~10 ±0.6 mm/yr oriented N41°W ±5°) and *Gordon et al.* [1993] (12.3 mm/yr ±0.6 mm/yr oriented N46°W ±3° for station OVRO, which is close to the Sierra Nevada). The principal differences among these models are in the assumptions of what stations define stable North America.

Sierra Nevada rotation. In order to cross the Sierra Nevada block, we first must estimate its rotation rate. Without well-constrained geologically based velocity estimates for the northern and southern Sierra Nevada, we obtain only rough limits. Perhaps a more useful approach is to use the rotation rate estimated by *Argus and Gordon* [1990, 1991], based on VLBI geodetic results. At 0.6°/m.y. counterclockwise, their rate is greater than our geologically inferred rate (which is indistinguishable from zero) yet still contributes relatively little influence on the net Pacific-North America velocity estimate. A rotation rate of 0.6°/m.y. yields a south directed velocity of 1.5 mm/yr for a path crossing the Sierra Nevada-Great Valley block. Because this estimate depends on the velocity of a geodetic site within the Owens Valley (OVRO) that excludes (low) rates of normal activity on the frontal range of the Sierra Nevada, we think that this estimate represents an upper limit of the rotation rate. To represent the effects of Sierra Nevada rotation, we choose a vector 1.0† +0.5-1.0† mm/yr oriented south† ±35°†.

Contraction near the San Andreas fault. We infer that little deformation is encountered in crossing the

Sierra Nevada and the San Joaquin Valley until the western margin of the San Joaquin Valley is encountered. Contraction north of the Transverse Ranges essentially perpendicular to the San Andreas fault is expressed by the presence of folds and earthquakes with reverse mechanisms like the 1983 Coalinga event and by offshore thrusting [*Crouch et al.*, 1984]. The best evidence for the magnitude of shortening comes from retrodeformable cross sections through the entire California coastal margin [*Namson and Davis*, 1988]. For this reason we include all of the San Andreas normal contraction in a single value derived from cross sections across the entire region. *Namson and Davis* [1988] report approximately 33 km of contraction along our path between the San Joaquin Valley and the Pacific plate, normal to the San Andreas fault. It is difficult for us to evaluate an uncertainty in net shortening from the reconstructions of Namson and Davis, but we infer it is minor relative to the associated large age uncertainty. *Namson and Davis* [1988] refer to the shortening as "late Cenozoic" but appear to prefer an initiation to the major phase of shortening near 2.3 Ma. This gives a rate that we believe is too great (~14 mm/yr). We infer from their sections that the deformation began in the late Miocene; this is supported by a late Miocene onset for shortening near the coast along a similar line [*Davis and McIntosh*, 1987]. Using an initiation date of 10 Ma, we get an estimated shortening rate of 3.3 mm/yr. However, it has also been suggested that much of the late Cenozoic shortening observed in a broad region of the Coast Ranges where our path crosses occurred when this country was in the vicinity of the Big Bend [*Weldon and Humphreys*, 1989]. Considering this, we choose a lower rate of 2† mm/yr as our most likely rate, and because of the uncertainty in the timing of deformation and the possibility that the Quaternary rate is greater the late Cenozoic average, we assign limits of +5† and -1.5† mm/yr. This allows, for instance, for 21 km of shortening progressing at a steady rate since 3 Ma. At the lower limit, shortening occurs at trivial rates. *Argus and Gordon* [1990, 1991] considered VLBI data from eastern California and the Pacific and concluded that only a few millimeters per year of contraction currently occurs in California west of the Sierra Nevada.

Mount and Suppe [1987], *Springer* [1987], and *Zoback et al.* [1987] report a direction of maximum compressive stress typically in the range of N40°E and N60°E. The orientation of shortening inferred from geologic structures in this region is ~N40°E [*Mount and Suppe*, 1987]. We assign an average value of N45°E† for the shortening direction. We include the range of estimated orientations from N40°E† and N60°E†.

Right-lateral shear on and near the San Andreas fault. Right-lateral shear across this portion of the path is dominated by the San Andreas and the Hosgri fault zones. However, there are two other zones of active seismicity between these zones [*Poley et al.*, 1987]. We divide the activity between the San Andreas, which is well defined, and an estimate of the net right-lateral shear to the west. Our path crosses the San Andreas fault at a place where the best available slip rate exists for the San Andreas fault in central California. *Sieh and Jahns* [1984] have documented a late Holocene slip rate of 34† ±3† mm/yr. This value is consistent with creep rates to the north [*Burford and Harsh*, 1980; *Schultz*, 1989] and geodetic estimates of the rate of strain accumulation [*Thacher*, 1979; *Savage*, 1983; *King et al.*, 1987]. The average trend of the San Andreas fault through this part of its course is N41°W† ±4°†.

Of the strike-slip faults to the west, only the San Simeon strand of the Hosgri fault system has well-documented late Quaternary slip rates. *Weber and Lajoie* [1977] reported a rate of 6 to 13 mm/yr. More recent studies of the same offset marine terraces suggest a lower rate of 4 mm/yr +6-2 mm/yr [*Hanson et al.*, 1992; *Hall et al.*, 1987]. Because the San Simeon fault is only one strand of the Hosgri zone and the Hosgri is only the most active of the faults west of the San Andreas, we infer a rate of 6† +6-4† mm/yr. The limits are based on the lowest and highest proposed rates for the San Simeon fault alone, but appear to be wide enough to encompass the entire deformation west of the San Andreas fault. The orientation of the Hosgri fault system at San Simeon is N40°W†, though individual traces deviate by ±15°†.

Convolving the probability distributions associated with this Sierra Nevada path results in an end-of-path vector of 48 ±4 mm/yr N41°W ±4° (at 90% confidence), which is shown in Figure 6.

Acknowledgments. We thank Andrew Griscom and James Savage for thoughtful and careful reviews. Don Argus, Tim Dixon, Roy Dokka, Ken Dueker, Richard Gordon, Randy Palmer, and Bob Powell are thanked for discussions about the nature and implications of deformation in the southwest U.S. We thank Don Argus and Tim Dixon for providing results on NUVEL-1A and Sierra Nevada motion (respectively) prior to publication. Beverly Effinger and Ann Blanchard converted our sketches into quality illustrations. This work occurred over many years, supported by grants 14-08-0001-G1780, 1434-92-G-2211 and 1434-93-G-2288 from the USGS, EAR-905714 from the NSF, and NAG 5-755 and NAG 5-1903 from NASA.

References

Allen, C. R., L. T. Silver, and F. G. Stehli, Agua Blanca fault: A major transverse structure of northern Baja California, Mexico, *Geol. Soc. Am. Bull.*, *71*, 457-482, 1960.

Anderson, J. G., Estimating the seismicity from geological structure for seismic-risk studies, *Bull. Seismol. Soc. Am.*, *69*, 135-158, 1979.

Anderson, R. E., T. P. Barnhard, Aspects of three-dimensional strain at the margin of the extensional orogen, Virgin River depression area, Nevada, Utah, and Arizona, *Geol. Soc. Am. Bull.*, *105*, 1019-1052, 1993.

Anderson, R. E., C. R. Longwell, R. L. Armstrong, and R. F. Marvin, Significance of K-Ar ages of Tertiary rocks from the Lake Mead region, Nevada/Arizona, *Geol. Soc. Am. Bull.*, *83*, 273-288, 1972.

Argus, D. F., and R. G. Gordon, Pacific-North America plate motion from very long baseline interferometry compared with motion inferred from magnetic anomalies, transform faults, and earthquake slip vectors, *J. Geophys. Res.*, *95*, 17,315-17,324, 1990.

Argus, D. F., and R. G. Gordon, Current Sierra Nevada-North America motion from very long baseline interferometry: Implications for the kinematics of the western United States, *Geology*, *19*, 1085-1088, 1991.

Astiz, L., and C. R. Allen, Seismicity of the Garlock fault, California, *Bull. Seismol. Soc. Am.*, *73*, 1721-1734, 1983.

Atwater, T., Implications of plate tectonics for the Cenozoic tectonic evolution of western North America, *Geol. Soc. Am. Bull.*, *81*, 3513-3536, 1970.

Barrows, A. G., J. E. Kahle, and D. J. Beebe, Earthquake hazard and tectonic history of the San Andreas fault zone, Los Angeles County, California, *Open File Rep. Calif. Div. Mines Geol., 851 85-10 LA*, 236 pp., 1985.

Bartley, J. M., A. F. Glazner, and E. R. Schermer, North-south contraction of the Mojave block and strike-slip tectonics in southern California, *Nature, 248*, 1398-1401, 1990.

Beanland, S., and M. M. Clark, The Owens Valley fault zone, eastern California, and surface rupture associated with the 1872 earthquake, *Seismol. Res. Lett., 32*, 32, 1987.

Biasi, G. P., and E. D. Humphreys, *P*-wave image of the upper mantle structure of central California and southern Nevada, *Geophys. Res. Lett., 19*, 1161-1164, 1992.

Bird, P., and J. Baumgardner, Fault friction, regional stress, and crust-mantle coupling in southern California from finite element models, *J. Geophys. Res., 89*, 1932-1944, 1984.

Bird, P., and R. W. Rosenstock, Kinematics of present crust and mantle flow in southern California, *Geol. Soc. Am. Bull., 95*, 946-957, 1984.

Bohannon, R. G., Strike-slip faults in the Lake Mead region of southern Nevada, in *Cenozoic Paleogeography of the Western United States, Pac. Coast Paleogr. Symp. 3*, edited by J. M. Armentrout et al., pp. 129-139, Society of Economic Paleontologists and Mineralogists, Pacific Section, Los Angeles, Calif., 1979.

Bohannon, G. G., Nonmarine sedimentary rocks of Tertiary age in the Lake Mead region, southeastern Nevada and northwestern Arizona, *U.S. Geol. Surv. Prof. Pap., 1259*, 69 pp., 1984.

Buising, A. V., Small-scale late Cenozoic faulting in the Colorado River extensional corridor, western Arizona and southeastern California, in *Deformation Associated With the Neogene Eastern California Shear Zone, Southeastern California and Southwestern Arizona, San Bernardino County, Spec. Publ. 92-1*, pp. 11-15, edited by S. M. Richard, San Bernardino County Museum, Redlands, Calif., 1992.

Burchfiel, B. C., and J. H. Stewart, The "pull-apart" origin of Death Valley, *Geol. Soc. Am. Bull., 77*, 439-442, 1966.

Burchfiel, B. C., K. V. Hodges, and L. H. Royden, Geology of Panamint Valley-Saline Valley pull-apart system, California, *J. Geophys. Res., 92*, 10,422-10,426, 1987.

Burford, R. O., and P. Harsh, Slip on the San Andreas fault in central California from alignment array surveys, *Bull. Seismol. Soc. Am., 70*, 1233-1261, 1980.

Butler, P. R., B. W. Troxel, and K. L. Verosub, Late Cenozoic history and styles of deformation along the southern Death Valley fault zone, *Geol. Soc. Am. Bull., 100*, 402-410, 1988.

Calderone, G. J., and R. F. Butler, Paleomagnetism of Miocene volcanic rocks from southwestern Arizona: Tectonic implications, *Geology, 12*, 627-630, 1984.

Calderone, G. J., G. D. Acton, and R. F. Butler, Concordant paleomagnetic directions from Miocene volcanic rocks, Colorado River region, Arizona and California (abstract), *Eos Trans. AGU, 67*, 922, 1986.

Calderone, G. J., R. F. Butler, and G. D. Acton, Paleomagnetism of middle Miocene volcanic rocks in the Mojave-Sonoran Desert region of western Arizona and southeastern California, *J. Geophys. Res., 95*, 625-647, 1990.

Carter, B. A., Quaternary displacement on the Garlock fault, California, in *Geology and Mineral Wealth of the California Desert, Dibblee Volume*, edited by D. L. Fife and A. R. Brown, pp. 457-465, South Coast Geological Society, Santa Ana, Calif., 1980.

Carter, B. A., Neogene displacement on the Garlock fault, California (abstract), *Eos Trans. AGU, 63*, 1124, 1982.

Carter, J. N, B. P. Luyendyk, and R. R. Terres, Neogene clockwise rotation of the eastern Transverse Ranges, California, suggested by paleomagnetic vectors, *Geol. Soc. Am. Bull., 98*, 199-206, 1987.

Chapin, C. E., Evolution of the Rio Grande Rift–A summary, in *Rio Grande Rift: Tectonics and Magmatism*, edited by R. E. Reicker, pp. 1-5, AGU, Washington, D. C., 1979.

Clark, M. M., and K. R. Lajoie, Holocene behavior of the Garlock fault, in Geological Survey Research 1974, *U.S. Geol. Surv. Prof., Pap., 900*, 184-185, 1974.

Clark, M. M., et al., Preliminary slip rate table and map of late Quaternary faults of California, *U.S. Geol. Surv. Open File Rep., 84-106*, 1984.

Crouch, J. K., S. B. Bachman, and J. T. Shay, Post Miocene compressional tectonics along the central California margin, in *Tectonics and Sedimentation Along the California Margin*, edited by J. K. Crouch and S. B. Bachman, pp. 37-54, Society of Economic Paleontologists and Mineralogists, Pacific Section, Los Angeles, Calif., 1984.

Crowell, J. C., and A. G. Sylvester (Eds.), *Tectonics of the Juncture Between the San Andreas Fault System and the Salton Trough, Southeastern California, A Guidebook for Fieldtrips*, Geological Society of America, Boulder, Colorado, 1979.

Davis, G. A. and B. C. Burchfiel, Garlock fault: An intra-continental transform structure, southern California, *Geol. Soc. Am. Bull., 84*, 1407-1422, 1973.

Davis, T. L., and K. D. McIntosh, A retrodeformable structural solution across the southern Coast Ranges and implications for seismically active structures, *Geol. Soc. Am. Abstr. Programs, 19*, 385, 1987.

DeMets, C., R. G. Gordon, D. F. Argus, and S. Stein, Current plate motions, *Geophys. J. Int., 101*, 425-478, 1990.

Dibblee, T. W., Jr., Aerial geology of the western Mojave Desert, California, *U.S. Geol. Surv. Prof. Pap., 522*, 153 pp., 1967.

Dibblee, T. W., Jr., Regional geology of the Transverse Ranges province of Southern California, in *Geology and Mineral Wealth of the California Transverse Ranges, Mason Hill Volume*, edited by D. L. Fife and J. A. Minch, pp.7-26, South Coast Geological Society, Santa Ana, Calif., 1982.

Dokka, R. K., Displacements on late Cenozoic strike slip faults of the central Mojave Desert, California, *Geology, 11*, 305-308, 1983.

Dokka, R. K., and C. J. Travis, Late Cenozoic strike-slip faulting in the Mojave Desert, California, *Tectonics, 6*, 311-240, 1990.

Donnellan, A., B. H. Hager, R. W. King, and T. A. Herring, Geodetic measurement of deformation in the Ventura Basin, southern California, *J. Geophys. Res., 98*, 21,727-21,739, 1993.

Eaton, G. P., R. R. Wahl, H. J. Prostka, D. R. Mabey, and M. D. Kleinkopf, Regional gravity and tectonic patterns: their relation to late Cenozoic epeirogeny and lateral spreading in the western Cordillera, in Cenozoic Tectonics and Regional Geophysics of the Western Cordillera, edited by R. B. Smith and G. P. Eaton, *Mem. Geol. Soc. Am., 152*, 51-92, 1978.

Eaton, J. E., Decline of the Great Basin, southwestern United States, *AAPG Bull., 16*, 1-49, 1932.

Eberhart-Phillips, D., M. Lisowski, and M. D. Zoback, Crustal strain near the Big Bend of the San Andreas fault: Analysis of the Los Padres-Tehachapi trilateration networks, California, *J. Geophys. Res., 95*, 12,139-12,153, 1990.

Elders, W. A., R. W. Rex, T. Meidav, P. T. Robinson, and S. Biehler, Crustal spreading in southern California: The Imperial Valley and the Gulf of California formed by rifting apart of a continental plate, *Science, 178*, 15-24, 1972.

Feigl, K. L., R. W. King, and T. H. Jordon, Geodetic measurement of tectonic deformation in the Santa Maria fold and thrust belt, California, *J Geophys. Res., 95*, 2679-2699, 1990.

Feigl, K. L, et al., Space geodetic measurement of crustal deformation in central and southern California, 1984-1992, *J. Geophys. Res., 12*, 21,677-21,712, 1993.

Frizzell, V. A., Jr., J. M. Mattison, and J. C. Matti, Distinctive Triassic megaporphyritc monzogranite: Evidence for only 160 kilometers of offset along the San Andreas fault, southern California, *J. Geophys. Res., 91*, 14,080-14,088, 1986.

Garfunkel, Z., Model for the late Cenozoic tectonic history of the Mojave Desert, California, *Geol. Soc. Am. Bull., 85*, 1931-1944, 1974.

Gillespie, A. R., Quaternary glaciation and tectonism in the southeastern Sierra Nevada, Inyo County, Cal., Ph.D. dissertation, 695 pp., Calif. Inst. of Technol., Pasadena, 1982.

Golombek, M. P., Geometry and rate of extension across the Pajarito fault zone, Espanola basin, Rio Grande rift, northern New Mexico, *Geology, 9*, 21-24, 1981.

Golombek, M. P., G. E. McGill, and L. Brown, Tectonic and geologic evolution of the Espanola basin, Rio Grande Rift: Structure, rate of extension, and relation to the state of stress in the western United States, *Tectonophysics, 94*, 483-507, 1983.

Gordon, D., C. Ma, and J. W. Ryan, Results from the CDP mobile VLBI program in the western United States, in *Contributions of Space Geodesy to Geodynamics, Geodyn. Ser.*, vol. 23, edited by D. E. Smith and D. L. Turcotte, pp. 131-138, AGU, Washington, D.C., 1993.

Greensfelder, R. W., F. C. Kintzer, and M. R. Somerville, Seismotectonic regionalization of the Great Basin, and comparison of moment rates computed from Holocene strain and historic seismicity, *U.S. Geol. Surv. Open File Rep., 80-801*, 433-493, 1980.

Greis, R., North-south compression of Rocky Mountain Foreland structures, in *Rocky Mountains Foreland Basins and Uplifts*, edited by J. D. Lowell, pp. 9-32, Rocky Mountain Association of Geologists, Denver, Colo., 1983.

Hall, N. T., T. D. Hunt, P. A. Vaughan, and F. R. Bickrer, Trenching of the San Simeon fault, San Luis Obispo County, California, *Geol. Soc. Am. Abstr. Programs, 19*, 385, 1987.

Hamblin, W. K., P. E. Damon, and W. B. Bull, Estimates of vertical crustal strain rates along the western margins of the Colorado Plateau, *Geology, 9*, 293-298, 1981.

Hamilton, W., Laramide crustal shortening, in Interaction of the Rocky Mountain Foreland and the Cordilleran Thrust Belt, edited by C. J. Schmidt and W. J. Perry, *Mem. Geol. Soc. Am., 171*, 27-39, 1988a.

Hamilton, W., Tectonic setting and variations with depth of some Cretaceous and Cenozoic structural and magmatic systems of the western United States, in *Metamorphic and Crustal Evolution of the Western United States, Ruby Volume VII*, edited by W. G. Ernst, pp. 1-40, Prentice-Hall, Englewood Cliffs, N. J., 1988b.

Hanson, K. L., W. R. Lettis, J. R. Wesling, K. I. Kelson, and L. Mezger, Quaternary marine terraces, south-central coastal California: Implications for crustal deformation and coastal evolution, in Quaternary Coasts of the United States: Marine and Lacustrine Systems, edited by C. H. Fletcher and J. F. Wehmiller, *Spec. Publ. Soc. Econ. Paleontol. Mineral., 48*, 323-332, 1992.

Hatch, M. E., and T. K. Rockwell, Neotectonics of the Agua Blanca fault, Agua Blanca valley, northern Baja California, Mexico, *Geol. Soc. Am. Abstr. Programs, 18*, 114, 1986.

Hauksson, E., and L. M. Jones, The July 1986 Oceanside (ML 5.3) earthquake sequence in the continental borderland, southern California, *Bull. Seismol. Soc. Am., 78*, 1885-1906, 1988.

Hauksson, E., and G. F. Saldivar, Seismicity and active compressional tectonics in Santa Monica Bay, southern California, *J. Geophys. Res., 94*, 9591-9606, 1989.

Hill, M. L., Anomalous trends of the San Andreas fault in the Transverse Ranges, California, in *Geology and mineral wealth of the California Transverse Ranges, Annu. Symp. Guideb., 10*, edited by D. L. Fife and J. A. Minch, pp. 367-369, South Coast Geological Society, Santa Ana, Calif., 1982.

Hirth, J. P., and J. Lothe, *Theory of Dislocations*, p. 293, John Wiley, New York, 1982.

Hornafius, J. S., Neogene tectonic rotation of the Santa Ynez Range, western Transverse Ranges, California, suggested by paloemagnetic investigation of the Monterey Formation, *J. Geophys. Res., 90*, 12,503-12,522, 1985.

Humphreys, E. D., and K. G. Dueker, Western U.S. upper mantle structure, *J. Geophys. Res., 99*, 9615-0634, 1994.

Humphreys, E. D., and B. H. Hager, A kinematic model for the late Cenozoic development of southern California crust and upper mantle, *J. Geophys. Res., 95*, 19,747-19,762, 1990.

Humphreys, E. D., and R. J. Weldon, Kinematic constraints on the rifting of Baja California, Chapter 12, in The Gulf and Peninsular Provinces of the Californias, edited by J. P. Dauphin and B. R. T. Simoneit, *AAPG Mem., 47*, 217-229, 1991.

Jackson, J., and P. Molnar, Active faulting and block rotations in the western Transverse Ranges, California, *J. Geophys. Res., 95*, 22,073-22,087, 1990.

Jennings, C. W., Fault map of California, with locations of volcanos, thermal springs, and thermal wells, scale 1:750,000, Calif. Div. of Mines and Geol., Sacramento, 1974.

Keller, E. A., M. S. Bonkowski, R. J. Korsch, and R. J. Shlemon, Tectonic geomorphology of the San Andreas fault zone in the southern Indio Hills, Coachella Valley, California, *Geol. Soc. Am. Bull., 93*, 46-56, 1982.

Kelley, V. C., Tectonics, middle Rio Grande rift, New Mexico, in *Rio Grande Rift: Tectonics and Magmatism*, edited by R. E. Reicker, pp. 57-70, AGU, Washington, D. C., 1979.

Kennedy, M. P., Recency and character of faulting along the Elsinore fault zone in southern Riverside County, California, *Calif. Div. Mines Geol. Spec. Rep. 131*, 12 pp., 1977.

King, N. E., P. Segall, and W. Prescott, Geodetic measurements near Parkfield, California, 1959-1984, *J. Geophys. Res., 92*, 2747-2766, 1987.

Legg, M. R., Fault character and seismotectonics along the western boundary of the southern California microplate (abstract), *Eos Trans. AGU, 69*, 1419, 1988.

Legg, M. R., Sea Beam evidence of recent tectonic activity in the California continental borderland, in The Gulf and Peninsular Provinces of the Californias, edited by J. P. Dauphin and B. R. T. Simoneit, *AAPG Mem., 47*, 179-196, 1991.

Legg, M. R., J. Mammerickx, B. P. Luyendyk, C. Demoustier, and R. C. Tyce, Seabeam survey of an active strike slip fault: The San Clemente fault in the California continental Borderland, *J. Geophys. Res., 94*, 1727-1744, 1989.

Legg, M. R., O. V. Wong, and F. Suarez, Geologic structure and tectonics of the inner continental borderland of northern Baja California, in The Gulf and Peninsular Provinces of the Californias, edited by J. P. Dauphin and B. R. T. Simoneit, *AAPG Mem., 47*, 145-177, 1991.

Liu, W., Paleomagnetism of Miocene sedimentary rocks in the Transverse Ranges; the implications for tectonic history, Ph.D. dissertation, 233 pp., Calif. Inst. of Technol., Pasadena, 1990.

Louie, J. N., C. R. Allen, D. C Johnson, P. C. Hasse, and S. N. Cohn, Fault slip in southern California, *Bull. Seismol. Soc. Am., 75*, 811-833, 1985.

Lubetkin, K. K. C., and M. M. Clark, Late Quaternary activity along the Lone Pine fault, eastern California, *Geol. Soc. Am. Bull., 100*, 755-766, 1988.

Luyendyk, B. P., M. J. Kamerling, and R. Terres, Geometric model for Neogene crustal rotations in southern California, *Geol. Soc. Am. Bull., 91*, 211-217, 1980.

Luyendyk, B. P., M. J. Kamerling, R. Terres, and J. S. Hornafius, Simple shear of southern California during Neogene time suggested by paleomagnetic declinations, *J. Geophys. Res., 90*, 12,454-12,466, 1985.

Matti, J. C., D. M. Morton, and B. F. Cox, Distribution and geologic relations of fault systems in the vicinity of the central Transverse Ranges, southern California, *U.S. Geol. Surv. Open File Rep., 85-865*, 27 pp., 1985.

Mayer, L., Topographic constraints on models of lithospheric stretching of the Basin and Range province, western United States, in Extensional Tectonics of the Southwestern United States: A Perspective on Processes and Kinematics, edited by L. Mayer, *Spec. Pap. Geol. Soc. Am., 208*, 1-14, 1986.

Meisling, K. E., and R. J. Weldon, Late Cenozoic tectonics of the northwestern San Bernardino Mountains, southern California, *Geol. Soc. Am., Bull., 101*, 106-128, 1989.

Menges, C. M., and P. A. Pearthree, Map of neotectonic (latest Pliocene-Quaternary) deformation in Arizona, *Open File Rep. 83-22*, Ariz. Bur. of Geol. and Min. Technol., Tucson, 1983.

Merifield, P. M., T. K. Rockwell, and C. C. Loughman, Slip rate on the San Jacinto fault zone in the Anza seismic gap, southern California, *Geol. Soc. Am. Abstr. Programs, 19*, 431-432, 1987.

Mills, G. and P. J. Fischer, Thrusting associated with offshore Newport-Inglewood-Rose Canyon zone, California, *Geol. Soc. Am. Abstr. Programs, 23*, 198, 1991.

Minster, J. B., and T. J. Jordan, Present-day plate motions, *J. Geophys. Res., 83*, 5331-5354, 1978.

Minster, J. B., and T. J. Jordan, Vector constraints on Quaternary deformation of the western United States east and west of the San Andreas fault, in *Tectonics and Sedimentation Along the California Margin* edited by J. K. Crouch and S. B. Bachman, pp. 1-16, Society of Economic Paleontologists Mineralogists, Pacific Section, Los Angeles, Calif. 1984.

Mount, V. S. and J. Suppe, State of stress near the San Andreas fault: Implications for wrench tectonics, *Geology, 15*, 1143-1146, 1987.

Namson, J., and T. L. Davis, Seismically active fold and thrust belt in the San Joaquin Valley, central California, *Geol. Soc. Am. Bull., 100*, 257-273, 1988.

Pacheco, J., and J. Nabelek, Source mechanisms of three moderate California earthquakes of July, 1986, *Bull. Seismol. Soc. Am., 78*, 1907-1929, 1988.

Pampeyan, E. H., T. L. Holzer, and M. M. Clark, Modern ground failure in the Garlock fault zone, Fremont Valley, California, *Geol. Soc. Am. Bull., 100*, 677-691, 1988.

Pearthree, P. A., Late Quaternary faulting and seismic hazard in southeastern Arizona and adjacent potions of New Mexico and Sonora, Mexico, *Open File Rep. 86-8*, Ariz. Bur. of Geol. and Min. Technol., Tucson, 1986.

Pearthree, P. A., C. M. Menges, and L. Mayer, Distribution, recurrence, and possible tectonic implications of late Quaternary faulting in Arizona, *Open File Rep. 83-20*, Ariz. Bur. of Geol. and Min. Technol., Tucson, 1983.

Pezzopane, S., and R. J. Weldon II, Tectonic role of active faulting in central Oregon, *Tectonics, 12*, 1140-1169, 1993.

Pinault, C. T., and T. K. Rockwell, Rates and sense of Holocene faulting on the Elsinore fault: further constraints on the distribution of dextral shear between the Pacific and North American plates, *Geol. Soc. Am. Abstr. Programs, 16*, 624, 1984.

Poley, C. M., J. P. Eaton, and A. G. Lindh, Recent seismicity of the central California region from San Francisco to the Transverse Ranges, *Geol. Soc. Am. Abstr. Programs, 19*, 440, 1987.

Ponti, D. J., J. A. Barron, A. M. Sarna-Wojcicki, M. L. Cotton, C. Hummon, and C. L. Schneider, Benthic foram biostratigraphy and the age of the Pico formation in the northern Los Angeles Basin: Potential problems for evaluating activity of blind thrust faults (abstract), *Eos Trans. AGU, 74* (43), Fall Meeting suppl., 434, 1993.

Powell, R. E., Geology of the crystalline basement complex, eastern Transverse Ranges, southern California: constraints on regional tectonic interpretation, Ph.D. dissertation, 441 pp., Calif. Inst. of Technol., Pasadena, 1981.

Powell, R. E., and R. J. Weldon, Evolution of the San Andreas fault, *Annu. Rev. Earth Planet. Sci., 20*, 431-468, 1992.

Prescott W. H., M. Lisowski, and J. C. Savage, Velocity field along the San Andreas fault in southern California (abstract), *Eos Trans. AGU, 68*, 1506, 1987.

Ramirez, V. R., Hungry Valley Formation: Evidence for 220 km of post Miocene offset on the San Andreas fault, in *Tectonics and Sedimentation Along the San Andreas Fault System*, edited by D. W. Anderson and M. J. Rymer, pp. 33-44, Pacific Section, Society of Economic Paleontologists and Mineralogists, Los Angeles, 1982.

Richard, S. M, and R. K. Dokka, Geology of the Packard Wells fault zone, southeastern California, in *Deformation Associated With the Neogene Eastern California Shear Zone, Southeastern California and Southwestern Arizona, San Bernardino County Spec. Publ. 92-1*, pp. 71-74, edited by S. M. Richard, San Bernardino County Museum, Redlands, Calif., 1992.

Richard, S. M., and D. R. Sherrod, and R. M. Tosdal, Cibola Pass fault, southwestern Arizona, in *Deformation Associated With the Neogene Eastern California Shear Zone, Southeastern California and Southwestern Arizona, San Bernardino County Spec. Publ. 92-1*, pp. 66-70, edited by S. M. Richard, San Bernardino County Museum, Redlands, Calif., 1992.

Rockwell, T. K., Soil chronology, geology and neotectonics of the north-central Ventura basin, California, Ph.D. dissertation, 424 pp., Univ. of Calif., Santa Barbara, 1983.

Rockwell, T. K., Neotectonics of the San Cayetano fault, Transverse Ranges, California, *Geol. Soc. Am. Bull., 100*, 500-513, 1988.

Rockwell, T. K., E. A. Keler, M. M. Clark, and D. L. Johnston, Chronology and rates of faulting of Ventura River terraces, California, *Geol. Soc. Am. Bull., 95*, 1406-1474, 1984.

Rockwell, T. K., E. A., Keller, and G. R. Dembroff, Quaternary rate of folding of the Ventura Avenue anticline, western Transverse Ranges, southern California, *Geol. Soc. Am. Bull., 100*, 850-858, 1988.

Rockwell, T. K., D. L. Lamar, R. S. McElwain, and D. E. Millman, Late Holocene recurrent faulting on the Glen Ivy North strand of the Elsinore fault, southern California, *Geol. Soc. Am. Abstr. Programs, 17*, 177, 1986a.

Rockwell, T. K., P. M. Merifield, and C. C. Loughman, Holocene activity of the San Jacinto fault in the Anza seismic gap, southern California, *Geol. Soc. Am. Abstr. Programs, 18*, 177, 1986b.

Rockwell, T. K., A. P. Thomas, A. L. Stenson, and R. Crisman, Active northeast trending left-lateral faults between the Elsinore and San Jacinto fault zones, southern California, *Geol. Soc. Am. Abstr. Programs, 21*, 135, 1989.

Rust, D. J., Radiocarbon dates for the most recent large prehistoric earthquake and for late Holocene slip rates: San Andreas fault in part of the Transverse Ranges north of Los Angeles, *Geol. Soc. Am. Abstr. Programs, 14*, 229, 1982.

Ryan, J. W., C. Ma, and D. S. Caprette, NASA space geodesy program–GSFC data analysis–1992, *NASA Tech. Memo. TM-104572*, 1993.

Salyards, S. L., Dating and characterizing late Holocene earthquakes using paleomagnetics, Ph.D. dissertation, 225 pp., Calif. Inst. of Technol., Pasadena, 1988.

Salyards, S. L., K. E Sieh, and J. L. Kirschvink, Paleomagnetic measurement of nonbrittle coseismic deformation across the San Andreas fault at Pallett Creek, *J. Geophys. Res., 97*, 12,457-12,470, 1992.

Sauber J., Geodetic measurements of deformation in California, *NASA Tech. Memo. TM-100732*, 212 pp., 1989.

Sauber, J., W. Thacher, and S. C. Solomon, Geodetic measurements of deformation in the central Mojave Desert, *J. Geophys. Res., 91*, 12,683-12,693, 1986.

Saucier, F., and E. Humphreys, Horizontal crustal deformation in southern California from joint models of geologic and very long baseline interferometry measurements, in *Contributions of Space Geodesy to Geodynamics, Geodyn. Ser.*, vol. 23, edited by D. E. Smith and D. L. Turcotte, pp. 139-176, AGU, Washington, D.C., 1993.

Saucier, F., E. Humphreys, and R. Weldon, Stress near geometrically complex faults: Application to the San Andreas fault at Cajon Pass, southern California, *J. Geophys. Res., 97*, 5081-5094, 1992.

Savage, J. C., Strain accumulation in western United States, *Annu. Rev. Earth Planet. Sci., 11*, 11-43, 1983.

Savage, J. C., Equivalent strike-slip earthquake cycles in half-space and lithosphere-asthenosphere Earth models, *J. Geophys. Res., 91*, 4873-4879, 1990.

Savage, J. C., and M. Lisowski, Deformation in the Owens Valley, California, *Bull. Seismol. Soc. Am., 70*, 1225-1232, 1980.

Savage, J. C., J. P. Church, and W. H. Prescott, Geodetic measurement of deformation in Owens Valley, California, *Bull. Seismol. Soc. Am., 65*, 865-874, 1975.

Savage, J. C., M. Lisowski, and W. H. Prescott, An apparent shear zone trending north-northwest across the Mojave Desert into Owens Valley, eastern California, *Geophys. Res. Lett., 17*, 2113-2116, 1990.

Schug, D. L., T. K. Rockwell, and M. E. Hatch, Slip rate estimate for the western reach of the Agua Blanca fault, Baja California, Mexico, *Geol. Soc. Am. Abstr. Programs, 19*, 448, 1987.

Schultz, S. S., Catalog of creep meter measurements in California from 1966 through 1988, *U.S. Geol. Surv. Open File Rep., 89-650*, 1989.

Schwartz, D. P., and K. Coppersmith, Fault behavior and characteristic earthquakes: Examples from the Wasatch and San Andreas fault zones, *J. Geophys. Res., 89*, 5681-5698, 1984.

Schwartz, D. P., and R. J. Weldon, Late Holocene slip rate on the Mojave segment of the San Andreas fault zone, California: Preliminary results (abstract), *Eos Trans. AGU, 67*, 906, 1986.

Sharp, R. V., San Jacinto fault zone in the Peninsular Ranges of southern California, *Geol. Soc. Am. Bull., 78*, 705-729, 1967.

Sharp, R. V., Variable rates of late Quaternary strike slip on the San Jacinto fault zone, Southern California, *J. Geophys. Res., 86*, 1754-1762, 1981.

Sheffels, B., and M. McNutt, Role of subsurface loads and regional compensation in the isostatic balance of the Transverse Ranges, California: Evidence for intracontinental subduction, *J. Geophys. Res., 91*, 6419-6431, 1986. (Correction, *J. Geophys. Res., 92*, 6444, 1987.)

Sieh, K., Slip rate across the San Andreas fault and prehistoric earthquakes at Indio, California (abstract), *Eos Trans. AGU, 67*, 1200, 1986.

Sieh, K. E., and R. Jahns, Holocene activity of the San Andreas fault at Wallace Creek, California, *Geol. Soc. Am. Bull., 95*, 883-896, 1984.

Smith, R. B., Seismicity, crustal structure, and intraplate tectonics of the interior of the western Cordillera, in Cenozoic Tectonics and Regional Geophysics of the Western Cordillera, edited by R. B. Smith and G. P. Eaton, *Mem. Geol. Soc. Am., 152*, 111-144, 1978.

Smith, R. B., and M. Sbar, Contemporary tectonics and seismicity of the western United States with emphasis on the Intermontain seismic belt, *Geol. Soc. Am. Bull., 85*, 1205-1218, 1974.

Springer, J. E., Stress orientations from wellbore breakouts in the Coalinga region, *Tectonics, 6*, 667-676, 1987.

Steiner, M. B., Rotation of the Colorado Plateau, *Tectonics, 5*, 649-660, 1986.

Stewart, J. H., Basin-range structure in western North America: A review, in Cenozoic Tectonics and Regional Geophysics of the Western Cordillera, edited by R. B. Smith and G. P. Eaton, *Mem. Geol. Soc. Am. 152*, 1-13, 1978.

Stewart, J. H., Tectonics of the Walker Lane belt, western Great Basin: Mesozoic and Cenozoic deformation in a zone of shear, in *Metamorphism and Crustal Evolution of the Western United States, Rubey Volume VII*, edited by W. G. Ernst, pp. 683-713, Prentice-Hall, Englewood Cliffs, N. J., 1988.

Sylvester, A. G., and R. R. Smith, Tectonic transpression and basement-controlled deformation in the San Andreas fault zone, Salton Trough, California, *AAPG Bull., 60*, 2081-2102, 1976.

Terres, R. R., Paleomagnetism and tectonics of the central and eastern Transverse Ranges, southern California, Ph.D. dissertation, Univ. of Calif., Santa Barbara, 1984.

Terres, R. R., and B. P. Luyendyk, Neogene tectonic rotation of the San Gabriel region, California, suggested by paleomagnetic vectors, *J. Geophys. Res., 90*, 12,467-12,484, 1985.

Thacher, W., Systematic inversion of geodetic data in central California, *J. Geophys. Res., 84*, 2283-2295, 1979.

Troxel, B. W., and L. A. Wright, Tertiary extensional features, Death Valley region, eastern California, in *Centennial Field Guide, 1*, edited by M. L. Hill, pp. 121-132, Geological Society of America, Boulder, Colo., 1987.

Tweto, O., The Rio Grande Rift system in Colorado, in *Rio Grande Rift: Tectonics and Magmatism*, edited by R. E. Reicker, pp. 33-56, AGU, Washington, D. C., 1979.

Vaughan, P., and T. K. Rockwell, Alluvial stratigraphy and neotectonics of the Elsinore fault zone at Agua Tibia Mountain, southern California, in *Neotectonics and Faulting in Southern California, Field Trip Guides 10, 12, 18*, compiled by P. L. Ehlig, pp. 177-191, Cordilleran Section Geological Society of America, Boulder, Colo., 1986.

Wallace, R. E., Patterns and timing of late Quaternary faulting in the Great Basin Province and relation to some regional tectonic features, *J. Geophys. Res., 89*, 5763-5769, 1984.

Ward, S. N., Pacific-North America plate motions: new results from very long baseline interferometry, *J. Geophys. Res., 95*, 21,965-21,981, 1990.

Weber, G. E., and K. R. Lajoie, Late Pleistocene and Holocene tectonics of the San Gregorio fault zone between Moss Beach and Point Ano Nuevo, San Mateo County, California, *Geol. Soc. Am., Abstr. Programs, 9*, 524, 1977.

Weldon, R. J., The late Cenozoic geology of Cajon Pass; implications for tectonics and sedimentation along the San Andreas fault, Ph.D. dissertation, 382 pp., Calif, Inst. of Technol., Pasadena, 1986.

Weldon, R. J., and E. D. Humphreys, A kinematic model of southern California, *Tectonics, 5*, 33-48, 1986.

Weldon, R. J., and E. D. Humphreys, Comment on "Structural transect of the western Transverse Ranges" by J. Namson and T. Davis, *Geology, 17*, 769-770, 1989.

Weldon, R. J., and K. E. Sieh, Holocene rate of slip and tentative recurrence interval for large earthquakes on the San Andreas fault in Cajon Pass, southern California, *Geol. Soc. Am. Bull., 96*, 793-812, 1985.

Weldon, R. J., and J. E. Springer, Active faulting near the Cajon Pass well, Southern California: Implications for the stress orientation near the San Andreas fault, *Geophys. Res. Lett., 15*, 993-996, 1988.

Weldon, R. J., D. S. Winston, J. L. Kirschvink, and D. W. Burbank, Magnetic stratigraphy of the Crowder Formation, Cajon Pass, Southern California, *Geol. Soc. Am. Abstr. Programs, 16*, 689, 1984.

Weldon, R. J., K. E. Meisling, and J. Alexander, A speculative history of the San Andreas fault in the central Transverse Ranges, California, in The San Andreas Fault System: Displacement, Palinspastic Reconstruction, and Geologic Evolution, edited by R. E. Powell et al. , *Mem. Geol. Soc. Am., 178*, 161-198, 1993.

Wells, R. E., and J. W. Hillhouse, Paleomagnetism and tectonic rotation of the lower Miocene Peach Springs Tuff, Colorado Plateau, Arizona, to Barstow, California, *Geol. Soc. Am., Bull., 101*, 846-863, 1989.

Wernicke, B., G. J. Axen, and J. K. Snow, Basin and Range extensional tectonics at the latitude of Las Vegas, Nevada, *Geol. Soc. Am., Bull., 100*, 1738-1757, 1989.

Winston, D. S., Magnetic stratigraphy of the Crowder Formation, southern California M.S. thesis, 100 pp., Univ. of South. Calif., Los Angeles, 1985.

Withjack, M. O., and W. R. Jamison, Deformation produced by oblique rifting, *Tectonophysics, 126*, 99-124, 1986.

Wright, L. A., J. K. Otton, and B. W. Troxel, Turtleback surfaces of Death Valley viewed as phenomena of extension, *Geology, 2*, 53-54, 1974.

Yeats, R. S., Quaternary flake tectonics of the California Transverse Ranges, *Geology, 9*, 16-20, 1981.

Yeats, R. S., Large-scale Quaternary detachments in Ventura Basin, southern California, *J. Geophys. Res., 88*, 569-583, 1983.

Yeats, R. S., Late Quaternary slip rate on the Oak Ridge fault, Transverse Ranges, California: Implications for seismic risk, *J. Geophys. Res., 93*, 12,137-12,149, 1988.

Yeats, R. S., Converging more slowly, *Nature, 366*, 299-301, 1993.

Yeats, R. S., and B. U. Haq, Deep-sea drilling off the Californias: Implications of leg 63, *Initial Rep. Deep Sea Drill. Proj., 63*, 949-961, 1981.

Yeats, R. S., G. J., Huftile, and F. B. Grigsby, Oak Ridge fault, Ventura fold belt, and the Sisar decollement, Ventura Basin, California, *Geology, 16*, 1112-1116, 1988.

Zhang, P., M. Ellis, D. B. Slemmons, and F. Mao, Right-lateral displacements and the Holocene slip rate associated with prehistoric earthquakes along the southern Panamint Valley fault zone: Implications for southern Basin and Range tectonics and coastal California deformation, *J. Geophys. Res., 95*, 4857-4872, 1990.

Ziony, J. I., and R. F. Yerkes, Fault slip-rate estimation for the Los Angeles region: Challenges and opportunities, *Earthquake Notes, 55*, 8, 1984.

Zoback, M. L., State of stress and modern deformation of the northern Basin and Range province, *J. Geophys. Res., 94*, 7105-7128, 1989.

Zoback, M. L., R. E. Anderson, and G. A. Thompson, Cenozoic evolution of the state of stress and style of tectonism of the Basin and Range province of western United States, *Philos. Trans. R. Soc. London A, 300*, 407-434, 1981.

Zoback, M. D., M. L. Zoback, V. S. Mount, J. Suppe, J. P. Eaton, J. H. Healy, D. Oppenheimer, P. Reasenberg, L. Jones, C. B. Raleigh, I. G. Wong, O. Scotti, and C. Wentworth, New evidence on the state of stress of the San Andreas fault system, *Science, 238*, 1105-1111, 1987.

E. D. Humphreys and R. J. Weldon II, Department of Geological Sciences, University of Oregon, Eugene, OR 97403. (e-mail: gene@newberry.uoregon.edu)

(Received July 29, 1993; revised March 28, 1994; accepted March 31, 1994.)